

1 **Effects of lower troposphere vertical mixing on simulated clouds and precipitation over the**
2 **Amazon during the wet season**

3
4 Xiao-Ming Hu^{1,2}, Yongjie Huang¹, Ming Xue^{1,2}, Elinor Martin², Yang Hong³, Mengye Chen³,
5 Hector Mayol Novoa⁴, Renee McPherson⁵, Andres Perez⁴, Isaac Yanqui Morales⁴,
6 Auria Julieta Flores Luna⁴
7

8 ¹ Center for Analysis and Prediction of Storms, University of Oklahoma, Norman, Oklahoma,
9 73072, USA

10 ² School of Meteorology, University of Oklahoma, Norman, Oklahoma, 73072, USA

11 ³ School of Civil Engineering and Environmental Engineering, University of Oklahoma,
12 Norman, Oklahoma, 73072, USA

13 ⁴ Universidad Nacional de San Agustín de Arequipa, Arequipa, Perú

14 ⁵ Department of Geography and Environmental Sustainability, University of Oklahoma, Norman,
15 Oklahoma, 73072, USA
16

17 Submitted to

18 *Journal of Geophysical Research-Atmospheres*

19 initially on 1/19/2023

20 2nd on 4/26/2023

21 revised on 5/31/2023 2:23 PM
22

23 Corresponding author address:

24 Drs. Xiao-Ming Hu (xhu@ou.edu), Ming Xue (mxue@ou.edu)

25 Hector Mayol Novoa (hnovoa@unsa.edu.pe),

26 Phone: (405) 325- 0402

27 Center for Analysis and Prediction of Storms, and School of Meteorology

28 University of Oklahoma

29 Norman, Oklahoma 73072, USA
30

31 **Key points:** (≤140 characters)

- 32
- 33 1. disentangle turbulence/cloud/precipitation processes over Amazon and reveal root cause
34 for sensitivity to PBL schemes using the WRF model.
 - 35 2. FT mixing becomes prominent in the presence of clouds, which in turn supports
36 maintenance of the FT clouds that would otherwise dissipate.
 - 37 3. Stronger vertical moisture relay transport in ACM2 PBL scheme supports thicker FT
38 clouds, leading to reduced heating and precipitation.
- 39
40
41

42 **Abstract**

43 Planetary boundary layer (PBL) schemes parameterize unresolved turbulent mixing
44 within the PBL and free troposphere (FT). Previous studies reported that precipitation simulation
45 over the Amazon in South America is quite sensitive to PBL schemes and the exact relationship
46 between the turbulent mixing and precipitation processes is, however, not disentangled. In this
47 study, regional climate simulations over the Amazon in January-February 2019 are examined at
48 process level to understand the precipitation sensitivity to PBL scheme. The focus is on two
49 PBL schemes, the Yonsei University (YSU) scheme, and the asymmetric convective model v2
50 (ACM2) scheme, which show the largest difference in the simulated precipitation. During
51 daytime, while the FT clouds simulated by YSU dissipate, clouds simulated by ACM2 maintain
52 because of enhanced moisture supply due to the enhanced vertical moisture relay transport
53 process: 1) vertical mixing within PBL transports surface moisture to the PBL top, and 2) FT
54 mixing feeds the moisture into the FT cloud deck. Due to the thick cloud deck over Amazon
55 simulated by ACM2, surface radiative heating is reduced and consequently the convective
56 available potential energy (CAPE) is reduced. As a result, precipitation is weaker from ACM2.
57 Two key parameters dictating the vertical mixing are identified, p , an exponent determining
58 boundary layer mixing and λ , a scale dictating FT mixing. Sensitivity simulations with altered p ,
59 λ , and other treatments within YSU and ACM2 confirm the precipitation sensitivity. The FT
60 mixing in the presence of clouds appears most critical to explain the sensitivity between YSU
61 and ACM2.

62
63 **Plain Language Summary** (≤ 200 words)

64 Predictions of weather and climate in terms of clouds and precipitation over the Amazon
65 in South America are quite uncertain. This uncertainty has been largely attributed to errors in the
66 planetary boundary layer (PBL) scheme, which represents turbulent mixing. A lack of
67 understanding of the relationship between turbulence, clouds, and precipitation processes
68 prevents us from improving PBL representation in models to achieve better weather and climate
69 simulations.

70 This study disentangles the turbulence/clouds/precipitation relationship, and identifies the
71 root cause of model errors in PBL schemes using regional climate simulations over the Amazon.

72 Two PBL schemes, the Yonsei University (YSU) scheme, and the asymmetric convective model
73 v2 (ACM2) scheme, are examined, which show the largest difference in the simulated
74 precipitation. The main difference between the two PBL schemes is the dissipation (YSU) or
75 maintenance (ACM2) of clouds during daytime above the boundary layer, which modulates
76 surface heating and consequently precipitation. The maintenance of a thick cloud deck over the
77 Amazon in ACM2, is caused by enhanced vertical transport of moisture from the surface to
78 above the boundary layer. Such an improved understanding of the
79 turbulence/clouds/precipitation relationship allow us to propose potential solutions to improve
80 PBL schemes in weather and climate models

81

82

83 **Keywords:** Clouds, precipitation, free troposphere vertical mixing, regional climate dynamical
84 downscaling

85

86

87 **1. Introduction**

88 Climate change can cause shifted weather patterns, more extreme weather events,
89 reduced water availability, change in agricultural patterns and increased exposure to disease
90 ([Langenbrunner et al., 2019](#); [Prein et al., 2017](#); [Vera et al., 2006b](#)) and other significant impacts
91 on society. Accurate simulation of regional climate and the development of adaptation strategies
92 and corresponding policies are critical. Global climate model (GCM) simulations are too coarse
93 to resolve local forcing and local weather, and their precipitation simulation is generally poor.
94 Cloud-resolving regional climate model (RCM) simulations have emerged in recent years for
95 dynamically downscaling global climate simulations and climate change responses at spatial
96 scales that are more useful for decision making ([Huang et al., 2023](#); [Liu et al., 2022](#); [Prein et al.,](#)
97 [2022](#); [Prein et al., 2015](#); [Prein et al., 2017](#); [Sun et al., 2016](#)). However, compared to mid-latitude
98 regions, the performance of RCM simulations in reproducing precipitation over tropical regions,
99 such as the Amazon in South America, is understudied ([Chakraborty et al., 2020](#); [Prein et al.,](#)
100 [2022](#); [Tai et al., 2021](#)).

101 Noontime and afternoon mesoscale convective systems (MCSs) are the main source of
102 precipitation over the Amazon and thus Amazonian precipitation has a single afternoon peak in
103 diurnal cycle ([Giangrande et al., 2017](#); [Giangrande et al., 2020](#); [Prein et al., 2022](#); [Wu et al.,](#)
104 [2021a](#)). Moist advection from the Atlantic Ocean by northeasterly trade winds during the austral
105 summer wet season (January - February) and zonal wind convergence are important for
106 precipitation over the Amazon rainforest ([Fu et al., 1999](#)) and cloud and turbulence processes
107 play critical roles in modulating precipitation in the region ([Barber et al., 2022](#); [Chakraborty et](#)
108 [al., 2020](#); [Chakraborty et al., 2018](#); [Prein et al., 2022](#); [Vilà-Guerau de Arellano et al., 2020](#);
109 [Wright et al., 2017](#)). The relationship between processes of clouds, turbulence, and precipitation
110 in the region remains to be disentangled and their modelling uncertainties and sensitivities need
111 to be understood to improve simulations ([Giangrande et al., 2017](#); [Giangrande et al., 2020](#); [Prein](#)
112 [et al., 2022](#)).

113 Simulated precipitation over the Amazon is sensitive to the planetary boundary layer
114 (PBL) scheme, but the root cause for such sensitivity and the cause-effect relationship remain to
115 be disentangled ([Prein et al., 2022](#)). Within typical weather and climate models, PBL schemes
116 parameterize unresolved turbulent mixing within the PBL and the free troposphere; the PBL
117 schemes are therefore critical for reproducing the bulk boundary layer structures and profiles in

118 the whole atmospheric column, as well as their subsequent effects on weather and climate
119 simulations. Many studies ([Gunwani & Mohan, 2017](#); [Hu et al., 2012](#); [Hu et al., 2013a](#); [Hu et al.,
120 2010a](#); [Hu et al., 2019](#); [Wang & Hu, 2021](#)) have evaluated the performance of various modern
121 PBL schemes, with most of them focusing on continental cloud-free PBL. Compared to
122 continental clear PBL, much less is known about the performance of PBL schemes in presence of
123 clouds ([Angevine et al., 2012](#); [Huang et al., 2013](#); [Supinie et al., 2022](#); [Valappil et al., 2023](#);
124 [Yang et al., 2019](#)).

125 PBL schemes can be classified into local and nonlocal schemes. Local schemes estimate
126 the turbulent fluxes at each point in a model from the mean atmospheric variables and/or their
127 gradients at that point, whereas nonlocal schemes include turbulent fluxes based on the
128 atmospheric variables and their variations over a deeper layer covering multiple model levels
129 through the PBL ([Cohen et al., 2015](#); [Hu et al., 2010a](#)). The assumption among local schemes
130 that fluxes depend solely on local values and local gradients of model state variables is least
131 valid under convective conditions when turbulent fluxes are dominated by large eddies that
132 transport fluid over longer distances ([Hu et al., 2010a](#)). Previous studies found that traditional
133 local schemes (e.g., Mellor–Yamada–Janjić (MYJ) or quasi-normal scale elimination (QNSE))
134 predict daytime continental boundary layers that are too cool and shallow; while schemes that
135 include non-local treatment, such as the asymmetrical convective model, version 2 ([ACM2,
136 Pleim, 2007a](#)), the Yonsei University (YSU, [Hong et al., 2006](#)) schemes and the more recently-
137 updated local scheme (e.g., Mellor–Yamada Nakanishi and Niino ([MYNN, Nakanishi & Niino,
138 2006](#))) predict deeper and warmer daytime continental boundary layers than MYJ and QNSE
139 ([Bright & Mullen, 2002](#); [Clark et al., 2015](#); [Coniglio et al., 2013](#)). Also, nonlocal PBL schemes
140 can reproduce the slightly stable upper convective boundary layer while local schemes often fail
141 to do so ([Hu et al., 2019](#); [Wang et al., 2016](#)).

142 Recent PBL development has started to use the mass flux (MF) approach that has been
143 commonly used in cumulus parameterization schemes for large-eddy nonlocal mixing together
144 with the eddy-diffusivity (ED) closure parameterizing local mixing, such as the MYNN-EDMF
145 scheme ([Angevine et al., 2010](#); [Olson et al., 2019a](#); [Olson et al., 2019b](#); [Pergaud et al., 2009](#)).
146 Note that MYNN-EDMF parameterizes specifically nonlocal mixing associated with shallow
147 cumulus clouds, thus a convective parameterization is still needed to parameterize deep
148 convection if the grid spacing is not fine enough to explicitly represent deep convection. Most

149 previous PBL modeling studies focus on treatments within the boundary layer while free-
150 troposphere treatments rarely receive much attention ([Hu et al., 2012](#); [Lu & Wang, 2019](#); [Zhu et](#)
151 [al., 2021](#); [Zhu et al., 2019](#)), likely because that free-troposphere turbulence is weak under clear
152 conditions and the impact of its parameterization on weather and climate simulations is regarded
153 as minor.

154 [Huang et al. \(2021\)](#) and [Huang et al. \(2023\)](#) conducted nested-domain RCM simulations
155 with grid spacings of 15 and 3 km over the Amazon with different physics schemes. It is found
156 that the simulated precipitation is most sensitive to PBL schemes with the YSU scheme
157 significantly overpredicting Amazonian precipitation and the ACM2 scheme predicting the
158 weakest precipitation. Extending the work of [Huang et al. \(2023\)](#), this study aims to understand
159 the precipitation sensitivity over the Amazon at a process level and identify the root cause for the
160 different model behaviors, with particular attention paid to the behaviors and effects of PBL
161 schemes in cloudy environments, and both inside and above the PBL. Effects of lower
162 troposphere vertical mixing on simulated clouds and precipitation over the Amazon will be
163 elucidated.

164 The rest of this paper is organized as follows: In section 2, precipitation data, model
165 configurations, and numerical experiment design are described. In section 3, clouds/precipitation
166 sensitivity to PBL schemes is diagnosed using simulations with YSU and ACM2 and their
167 variants with altered turbulence treatments, followed by discussion of such sensitivity at a finer
168 resolution. Meanwhile the turbulence/cloud/precipitation processes over the Amazon are
169 examined. Finally, section 4 contains a summary and discussion of the main findings.

170

171 **2. Precipitation data, model configuration and numerical experiment design**

172 a) Precipitation data

173 Two gridded global precipitation datasets are used in this study to compare with
174 simulations, including (1) half-hourly Integrated Multi-satellitE Retrievals for GPM (IMERG) at
175 a horizontal resolution of $0.1^\circ \times 0.1^\circ$ ([Huffman et al., 2019](#)), and (2) half-hourly National
176 Oceanic and Atmospheric Administration (NOAA) Climate Prediction Center (CPC)
177 MORPHing Technique (CMORPH) global precipitation analyses at a horizontal resolution of ~ 8
178 km ([Joyce et al., 2004](#)).

179

180 b) Model configurations

181 [Huang et al. \(2021\)](#) and [Huang et al. \(2023\)](#) used the Weather Research and Forecasting
182 (WRF) model Version 4.2.1 ([Skamarock & Klemp, 2008](#); [Skamarock et al., 2021](#)) to perform
183 historical simulations over South America during January-February 2019 in preparation for
184 future regional climate dynamic downscaling. The simulations used hourly European Centre for
185 Medium-Range Weather Forecasts Reanalysis v5 ([ERA5, Hersbach et al., 2020](#)) for initial and
186 boundary conditions. Two one-way nested domains with 15- and 3-km horizontal grid spacings
187 cover the entire South America and the Peruvian central Andes region, respectively (see Fig. 1a
188 for domain coverage). Both domains use 61 stretched vertical levels topped at 20 hPa. Following
189 previous dynamic downscaling practices ([Hu et al., 2018](#); [Miguez-Macho et al., 2004, 2005](#);
190 [Wang & Kotamarthi, 2013](#)), spectral nudging technique is applied to the outer 15-km domain to
191 maintain large-scale circulations at a 1500 km scale, while allowing WRF to evolve smaller-
192 scale dynamics and physics. Twelve sensitivity experiments were conducted by [Huang et al.](#)
193 [\(2023\)](#) with varied PBL, microphysics schemes, and land surface models while other physics
194 parameterizations were kept the same among the sensitivity experiments, including revised MM5
195 Monin-Obukhov surface layer scheme ([Jiménez et al., 2012](#)), and the Rapid Radiative Transfer
196 Model for GCMs (RRTMG) longwave and shortwave radiation scheme ([Iacono et al., 2008](#)).
197 The Tiedtke cumulus parameterization scheme ([Tiedtke, 1989](#)) is used on the 15-km outer
198 domain to handle both shallow and deep convections but not on the 3-km inner domain.

199 These WRF downscaling simulations are found to be most sensitive to PBL schemes with
200 the YSU scheme significantly overpredicting Amazonian precipitation, the ACM2 scheme
201 predicting the weakest precipitation, and the MYNN-EDMF prediction being in the middle.
202 Such relative differences are maintained with altered microphysics schemes and land surface
203 models (LSMs). Simulations with the Thompson microphysics scheme ([Thompson et al., 2008](#)),
204 and the Noah LSM ([Chen & Zhang, 2009](#)) are chosen to investigate PBL sensitivities in this
205 study. Diagnosing the root cause for the differences between the YSU and ACM2 PBL schemes
206 and disentangle the impact of PBL schemes on precipitation are the foci of this study. Since
207 simulated precipitation is quite sensitive to some other parameterization, such as cumulus
208 schemes ([Hu et al., 2018](#)), and there are large uncertainties among different precipitation data
209 ([Chen et al., 2022](#)), recommending an optimal PBL scheme in terms of reproducing precipitation
210 is beyond the scope of this study, which may require more advanced profile measurements (e.g.,

211 cloud water profile) and more accurate precipitation data to justify as will be seen in our later
212 analyses.

213

214 c) Sensitivity simulations with altered treatments in ACM2 and YSU

215 In addition to the simulations conducted by [Huang et al. \(2023\)](#), eight more sensitivity
216 simulations (summarized in Table 1) are run to help identify the root cause of the differences
217 between ACM2 and YSU, and resolution dependence of the differences, as well as to examine
218 impact of turbulent processes on cloud and precipitation processes. ACM2 and YSU differ in
219 their treatments in both PBL and free troposphere. Sensitivity simulations adjusting either PBL
220 or free-troposphere mixing treatments or both are conducted.

221 In the PBL, while a counter-gradient term is added to the eddy diffusion equation to
222 handle nonlocal mixing in YSU, ACM2 explicitly simulates the transient nonlocal mass flux.
223 For the local mixing in the PBL, both ACM2 and YSU use a polynomial function/profile ([so
224 called K-profile, Noh et al., 2003](#)) to define the vertical mixing coefficient K_z for temperature
225 and moisture as:

$$226 \quad K_z = Pr^{-1} k \frac{u_*}{\phi} z \left(1 - \frac{z}{h}\right)^p \quad (1)$$

227 where Pr is the Prandtl number, k is the von Karman constant, ϕ is the similarity profile function,
228 z is the height above ground level, and h is the PBL height. Thus, ACM2 and YSU are also
229 categorized into the K -profile PBL schemes ([Hu et al., 2019](#)). In YSU and ACM2, the value of
230 the exponent p in (1) is set to 2 by default, but its optimal value may vary from 0.5 to 3
231 depending on flow conditions, with a larger/smaller p yielding smaller/larger K_z ([Hu et al., 2018](#);
232 [Hu et al., 2010b](#); [Nielsen-Gammon et al., 2010](#); [Troen & Mahrt, 1986](#)). While a similar local
233 mixing treatment is adopted in ACM2 and YSU, there are many differences in their parameter
234 values, profile functions, methods to diagnose PBL height, etc. ACM2 generally simulates
235 stronger vertical mixing in the PBL and higher PBL height under clear conditions ([Hu et al.,
236 2010a](#)). Since p effectively dictates the vertical mixing within the PBL, p is varied in sensitivity

237 simulations to understand model differences and physics processes including turbulence, clouds,
238 and precipitation (see experiment YSU. 5 in Table 1).

239 In the free troposphere, only local mixing is considered in YSU and ACM2 ([Hong, 2010](#);
240 [Nielsen-Gammon et al., 2010](#); [Pleim, 2007b](#)). Both YSU and ACM2 compute the K_z as a
241 function of mixing length l , vertical wind shear S , and the stability function $f(Ri)$:

$$242 \quad K_z = l^2 S f(Ri), \quad (2)$$

243 in which

$$244 \quad \frac{1}{l} = \frac{1}{kz} + \frac{1}{\lambda}, \quad (3)$$

245 where Ri is the Richardson number, and λ is the asymptotic length scale. Such first-order
246 parameterizations of turbulent vertical mixing are widely used in operational numerical weather
247 prediction (NWP) and climate models ([Beare et al., 2006](#); [Cuxart et al., 2006](#)). ACM2 and YSU
248 differ in their parameter values, Ri calculation within clouds, and stability functions. Both
249 ACM2 and YSU use moist-air Ri calculation adapted from [Durran and Klemp \(1982\)](#), but YSU
250 requires two layers of clouds to activate the moist-air Ri calculation between the two layers
251 while ACM2 only requires one layer, in addition to other differences in parameters. Note that
252 these PBL parameterizations only consider local in-cloud turbulent mixing, non-local in-cloud
253 mixing needs to be accounted for by a cumulus parameterization scheme on the convection-
254 parameterized grid or explicitly resolved by the convection-permitting grid. Much of the
255 improvement to such parameterizations (Eqs. 2-3) in NWP and climate models involved
256 adjusting the stability functions (for example short vs. long-tailed functions) and λ ([Cuxart et al.,](#)
257 [2006](#)). λ is adjustable and varies between 30 and 250 m in numerical models ([Cuxart et al., 2006](#);
258 [Liu & Carroll, 1996](#); [Nielsen-Gammon et al., 2010](#)). λ is set to 30 m in the YSU scheme and to
259 80 m in the ACM2 scheme. Sensitivity simulations are conducted in this study by replacing the
260 whole free-troposphere treatments (experiment YSUuseACM2free in Table 1) or only altering the
261 value of λ (experiment ACM2 λ 30 in Table 1).

262 The sensitivity simulations are conducted with the outer 15 km domain because the
263 difference between inner-domain outputs from our nested-domain runs with different
264 configurations are rooted from the different simulations in the outer 15km domain, as we will see
265 in our analysis. Thus, the conclusions from these sensitivity simulations have implications for
266 regional and global models that run at convection-parameterized resolutions. In addition, four

267 sensitivity simulations with a single domain covering the majority of the Amazon with a 3 km
268 grid spacing (experiments 3kmYSU, 3kmYSUp.5, 3kmYSUp.5useACM2free, 3kmACM2 in Table 1)
269 are also conducted to examine the applicability of conclusions obtained at 15 km grid spacing to
270 convection-allowing simulations.

271

272 **3. Results**

273 a) Cause of precipitation differences simulated with different PBL schemes

274 As stated earlier, WRF simulations over South America during January-February 2019
275 are conducted with 12 different physics schemes, including PBL, microphysics schemes and land
276 surface models ([Huang et al., 2023](#)). The simulated precipitation is most sensitive to PBL
277 schemes ([Huang et al., 2023](#)) with the YSU scheme predicting the strongest daily precipitation
278 rate while the ACM2 scheme predicting the weakest precipitation over the Amazon during the
279 summer wet season (Fig. 1). The relative strength of simulated precipitation between ACM2 and
280 YSU remains across different resolutions, including the convection-parameterized (15 km grid
281 spacing) and convection-permitting (3 km grid spacing) resolutions. The precipitation rate
282 increases with increased resolution. The YSU runs at 3 km grid spacing (including the nested run
283 focusing on Peru and the single-domain run focusing more on the Amazon) significantly
284 overestimate daily precipitation rate (Figs. 1c-f). The South America Affinity Group
285 (SAAG) led by National Center for Atmospheric Research (NCAR) also reported that a WRF
286 simulation using the YSU scheme at a grid spacing of 4 km over South America overestimated
287 precipitation over the Amazon ([Liu et al., 2022](#)).

288 Precipitation over the Amazon is dominated by mid-day and afternoon MCSs
289 ([Giangrande et al., 2017](#); [Giangrande et al., 2020](#); [Prein et al., 2022](#); [Wu et al., 2021a](#)). [Huang et](#)
290 [al. \(2021\)](#) and [Huang et al. \(2023\)](#) evaluated the simulated diurnal variation of precipitation. All
291 WRF simulations with different configurations reproduce the afternoon precipitation peak with
292 biases in intensity and timing. ACM2 scheme shows the best agreement with observations and
293 the difference between different PBL schemes are most significant in the afternoon (Fig. 2).
294 Thus, we will focus on the precipitation and related processes during daytime. During mid-day
295 hours, YSU simulates stronger hourly precipitation rates than ACM2 and overestimates
296 precipitation at both resolutions and over different domains (Figs. 2, 3).

297 Causative factors for the different precipitation simulated by ACM2 and YSU over the
298 Amazon are herein investigated. The impact of different PBL schemes on NWP and climate
299 simulations is more straightforward under clear conditions while their impacts on precipitation is
300 less clear. Often the impact of PBL schemes on precipitation is not conclusive because the
301 schemes produce different (stronger or weaker) precipitation in different cases ([Bright & Mullen,
302 2002](#); [Cohen et al., 2015](#); [Gopalakrishnan et al., 2023](#); [Jankov et al., 2005](#); [Jankov et al., 2007](#); [Li
303 & Pu, 2008](#); [Supinie et al., 2022](#); [Wu et al., 2021b](#); [Zhang et al., 2013](#)). Under clear conditions,
304 ACM2 simulates stronger boundary layer vertical mixing and deeper PBL than YSU due to
305 different treatments for nonlocal fluxes and different parameters/functions in the *K*-profile local
306 mixing ([Hu et al., 2010a](#); [Nielsen-Gammon et al., 2010](#); [Shin & Hong, 2011](#); [Xie et al., 2012](#)).
307 How such differences translate to significantly different precipitation with the two schemes is
308 the main question to be answered in this study.

309 Surface temperature shows distinct differences over the Amazon with the ACM2
310 simulating lower continental temperatures than YSU by 0.5-0.8 °C over the simulation domains
311 around noon (Fig. 4), which likely leads to less surface energy to feed MCSs. The lower
312 temperature simulated by ACM2 covers the main precipitation region over the Amazon (Fig. 4g)
313 and can likely explain the precipitation difference. However, such temperature differences
314 cannot be explained by the direct impact of PBL mixing. Prior work has shown that during
315 daytime, ACM2 simulates stronger mixing in the PBL and stronger PBL-free troposphere
316 exchange generally warming up the PBL due to entrainment of free troposphere air with higher
317 potential temperature ([Hu et al., 2010a](#); [Shin & Hong, 2011](#)). Thus, the direct impact of ACM2
318 PBL mixing should lead to higher surface temperature, rather than the lower temperature
319 obtained in the regions of precipitation.

320 Rather, the temperature difference between ACM2 and YSU simulations is more directly
321 related to the difference in surface downward shortwave radiation. ACM2 simulates less
322 shortwave radiation at the surface over the Amazon region (Fig. 5g), where cloud coverage is
323 significant (Fig. 5j). At 17 UTC (12-14 LST across south America), the average surface
324 shortwave radiation simulated by ACM2 is lower by $\sim 70 \text{ W m}^{-2}$ than the YSU runs. Thus, the
325 lower temperature simulated by ACM2 should be due to indirect effects of vertical mixing via
326 interactions with clouds and radiation.

327 Significant cloud coverage over the Amazon ([Kay et al., 2016](#); [Kay et al., 2012](#)) is a
328 characteristic distinguishing this study from most other studies of PBL schemes. Over the
329 Amazonian region, ACM2 simulates a thicker cloud deck (Fig. 6,7), which reduces downward
330 shortwave radiation (Fig. 8), consequently leading to a lower surface temperature. As a result,
331 the surface-based convective available potential energy (CAPE) is lower in the ACM2
332 simulations (Fig. 9), which would lead to weaker daytime precipitation. The significant
333 difference between YSU and ACM2 is mostly confined over the cloud region (Fig. 5 & 8), which
334 further confirms that indirect effects of vertical mixing over the Amazon via interactions with
335 clouds dominate its direct effects.

336 The cloud deck over the Amazon therefore appears to be a critical link to disentangle the
337 impact of PBL schemes on simulated precipitation. The low-level clouds are produced by
338 shallow convections and mid-level clouds are produced by deep convections either from isolated
339 convective towers typically in daytime or from propagating MCS typically during nighttime.
340 During daytime, while the clouds simulated with the YSU scheme dissipate gradually from the
341 early morning maxima, clouds simulated with the ACM2 scheme are still sustained through the
342 day (see cloud cross-sections at 11 - 21 UTC in Fig. 6). Daytime cloud thinning is likely due to
343 solar heating under condition of lack of water vapor supply available for condensation ([Adebiyi
344 et al., 2020](#); [Burleyson & Yuter, 2015](#); [Painemal et al., 2015](#); [Zhang et al., 2010](#)). The thicker
345 cloud deck simulated by ACM2 appears to be due to enhanced supply of boundary layer
346 moisture to the layers above (Fig. 10a), thus less boundary layer moisture by 0.6 g kg^{-1} and more
347 free troposphere moisture by 0.2 g kg^{-1} compared to the YSU run (Fig. 10b), through enhanced
348 boundary layer vertical mixing ([Hu et al., 2010a](#); [Shin & Hong, 2011](#)).

349 In the nested-domain simulations, surface temperature simulated by ACM2 is lower than
350 YSU in both 15 and 3 km domains (Fig. 4) and the resulting lower precipitation occurs in both
351 domains. The root cause of lower surface temperatures from ACM2 in the nested 3 km domain
352 is less clear due to the possible effect of 15 km simulations via advection through its lateral
353 boundaries. Thus, the main discussions below (in section b) will focus on further investigation
354 of PBL-clouds-precipitation relationship in the outer 15 km domain with additional simulations
355 with altered treatments, while their relationship at the convection-permitting resolution will be
356 examined with additional single-domain simulations with a 3 km grid spacing (in section c).

357

358 b) Impact of different turbulence treatments on clouds and precipitation

359 Lower troposphere turbulence plays important roles in cloud production and maintenance
360 ([Lilly, 1968](#)). This section discusses results of sensitivity simulations adjusting turbulence
361 treatments in YSU and ACM2. Since under clear conditions, ACM2 has stronger daytime
362 boundary layer mixing than YSU ([Hu et al., 2010a](#); [Shin & Hong, 2011](#)), vertical mixing in the
363 YSU PBL scheme is first enhanced to see if the simulated clouds and precipitation would
364 become closer to those simulated by ACM2. The exponent p in the K -profile in YSU (default
365 value is 2) is reduced to 0.5 in experiment YSU_{p=0.5} to enhance daytime boundary layer mixing, as
366 indicated by the K_z profiles in Fig. 10d. With $p=0.5$, YSU_{p=0.5} simulates higher PBL top height
367 (Fig. 10d). As a result, more near-surface moisture is transported to the top of the elevated PBL,
368 where a thicker cloud layer near the PBL top forms (Fig. 7c & Fig. 10c). Note that while the
369 nonlocal mixing is proportional to K_z in YSU, transient nonlocal fluxes are explicitly simulated
370 by ACM2, which is not shown in Fig. 10. Thus K_z profiles in Fig. 10d are more indicative of
371 total mixing in the boundary layer for YSU, but less so for ACM2. In the free troposphere where
372 there are no nonlocal mixing treatments for either scheme, thus K_z profiles are indicative of free-
373 troposphere mixing for both.

374 As the PBL grows in the daytime, the PBL top clouds simulated by both YSU and ACM2
375 keep elevating (Fig. 6). A more prominent/distinct PBL top cloud layer is simulated by YSU
376 (Fig. 6c,e, PBL top is marked by black dash lines) while the PBL top clouds simulated by ACM2
377 are indistinctive from the free-troposphere clouds (Fig. 6d,f). Existence of a PBL top cloud layer
378 over the Amazon was previously illustrated by cloud frequency data observed during the
379 GoAmazon 2014/5 field experiments ([Giangrande et al., 2017](#); [Giangrande et al., 2020](#)).
380 However, that dataset only provides cloud frequency, not cloud amount. To quantitatively verify
381 the simulated PBL top cloud layer, more advanced cloud dataset is needed.

382 The thickened PBL top clouds simulated by YSU with $p=0.5$ weakens surface shortwave
383 radiation (Fig. 8) and consequently lowers surface temperature and CAPE (Fig. 9), thus reduces
384 precipitation (Fig. 11). Such a precipitation sensitivity to boundary layer mixing over the
385 Amazon is consistent with that reported over the eastern United States ([Hu et al., 2018](#)).
386 However, YSU with $p=0.5$ does not reduce precipitation to the level simulated by ACM2 (Fig.
387 11). In comparison, ACM2 simulates a more prominent cloud layer at a higher elevation (~4-5
388 km above ground) while the clouds simulated by YSU at this altitude (with both default p value

389 and $p=0.5$) weaken in time during the day (Fig. 6). Thus, boundary layer mixing alone cannot
390 completely explain the different impacts of ACM2 and YSU on clouds.

391 In addition to the different treatments within the boundary layer, ACM2 and YSU also
392 differ in their treatments in the free troposphere. A YSU sensitivity simulation using ACM2's
393 free-troposphere mixing treatment (named YSUuseACM2free) is conducted to examine the
394 impact of free troposphere mixing. YSUuseACM2free simulates a stronger vertical mixing up to
395 7-8 km above the ground, particularly in the presence of clouds, similar to the ACM2 simulation
396 (Fig. 10d). In the absence of clouds, the free-troposphere mixing simulated by different PBL
397 schemes are all similar and weak (Figure S1 in Supporting Information). Higher aloft (>8 km),
398 ice and snow clouds dominate and peak in the afternoon (likely due to detrainment of deep
399 convection), and the sensitivity of vertical mixing is small and K_z is simulated to be mostly less
400 than $1 \text{ m}^2 \text{ s}^{-1}$ by all schemes. Thus, our analysis focuses on the lower free troposphere. As a
401 result of stronger mixing in the lower free troposphere, a thicker cloud deck at 4-5 km above
402 ground (Fig. 7d), similar to ACM2 (Fig. 7b), develops in the simulation, due to stronger moisture
403 supply from the PBL top (Fig. 10a). Consequently, surface temperature is reduced due to cloud
404 shield, and the precipitation is reduced, to be closer to that of ACM2 than YSU $p.5$ (Fig. 11).
405 Combining both $p=0.5$ and ACM2's free-troposphere mixing, YSU $p.5$ useACM2free simulates a
406 similar, but slightly thicker cloud deck (Fig. 7e) and slightly weaker precipitation than
407 YSUuseACM2free (Fig. 11). The mean free-troposphere clouds over Manaus (Fig. 10c)
408 simulated by YSU, YSU $p.5$, YSUuseACM2free, YSU $p.5$ useACM2free, ACM2 are 15.4, 17.5, 62.6,
409 73.7, 72.4 mg kg^{-1} respectively, among which the ones using ACM2's free-troposphere treatment
410 are grouped together. Different clouds are the net results of the different K_z , which is as large as
411 a factor of >20 in the free troposphere in the presence of clouds. These experiments illustrate
412 that free-troposphere mixing is the most critical difference between YSU and ACM2 in terms of
413 simulating clouds and precipitation, while the mixing in the PBL plays a secondary role.

414 For free troposphere vertical mixing, ACM2 and YSU differ in their parameters, moist-
415 air Ri calculation, and the stability functions. Previous studies identified λ as a critical parameter
416 for free-troposphere mixing ([Cuxart et al., 2006](#); [Hu et al., 2012](#); [Nielsen-Gammon et al., 2010](#)),
417 and here its impact is further examined. An ACM2 sensitivity simulation with $\lambda=30$ (named
418 ACM2 $\lambda30$) is conducted to verify its impact on clouds/precipitation. Comparing to default
419 ACM2 with $\lambda=80$, ACM2 $\lambda30$ simulates a much weaker mixing in the free troposphere (Fig. 10d),

420 and consequently a much thinner cloud deck at 4-5 km above ground and meanwhile the PBL
421 top clouds appear thicker (Fig. 7f), due to weaker vertical transport of moisture from the PBL top
422 to higher levels (Fig. 10a). The net result is that the surface radiation is enhanced (Fig. 8f),
423 temperature is higher, and more precipitation is produced (Fig. 11f). The precipitation simulated
424 by ACM2 λ 30 is not as strong as that simulated by YSU because of other differences in free-
425 troposphere and PBL mixing treatments.

426 All the above results together suggest a prominent *PBL-free-troposphere moisture relay*
427 *transport process*: Step 1, boundary layer mixing transports moisture to the PBL top where
428 clouds form; step 2, free-troposphere mixing transports the moisture further to higher levels (~ 4-
429 5 km) to sustain a thick cloud deck at that altitude and reduce the boundary layer top clouds
430 somewhat. *ACM2 simulates a strong PBL-free-troposphere moisture relay transport process.*
431 Comparing to YSU, ACM2 simulates less PBL moisture (by 0.5 g kg⁻¹) and more free
432 troposphere moisture (by 0.2 g kg⁻¹ at 3-6.5 km above ground, Fig. 10b) in monthly average.
433 Consequently, the free-troposphere cloud layer is better maintained during daytime. In contrast,
434 the moisture relay transport process simulated by YSU is weaker and the clouds at ~ 4-5 km
435 dissipate quicker during daytime, leading to less cloud coverage, more CAPE and
436 precipitation. Modified YSU with enhanced PBL and free-troposphere mixing
437 (YSUp.5useACM2free) produces similar moisture transport as ACM2 (Fig. 10b,d) hence reduced
438 precipitation. These results suggest that free-troposphere mixing may become prominent in the
439 presence of clouds (which otherwise would be weak as generally regarded) and become an
440 important step in the relay transport process. To verify the strength of such relay transport
441 process, more advanced observations, such as long-term vertical profiles of cloud mixing ratios,
442 are warranted. Our results also suggest that to correctly simulate clouds/precipitation in
443 environments similar to those of the Amazon, the ability of models in reproducing such moisture
444 relay transport processes needs to be carefully assessed.

445
446 c) Sensitivity of clouds and precipitation to different turbulence treatments at a convection-
447 allowing resolution

448
449 The sensitivity of simulated clouds and precipitation to boundary layer and free-
450 atmosphere vertical mixing discussed above is mainly based on simulations at 15 km grid
451 spacing where cumulus parameterization is employed. Thus, the conclusions are directly

452 applicable to global and regional weather and climate simulations/predictions at convection-
453 parameterized resolutions. Whether these conclusions are still valid at convection-permitting
454 resolutions requires additional examination. To avoid the possible effects of the driving 15 km
455 grid on the nested 3 km grid, single-domain sensitivity simulations are conducted that cover a
456 majority of the Amazon with a 3 km grid spacing that use ERA5 data directly as lateral boundary
457 conditions. These simulations include 3kmYSU, 3kmYSUp.5, 3kmYSUp.5useACM2free, and
458 3kmACM2 (as summarized in Table 1). Even though simulated precipitation rate is generally
459 higher at the 3 km grid spacing than at 15 km grid spacing, the same turbulent mixing → clouds
460 → precipitation impact/sensitivity holds in these convection-permitting simulations (Fig. 12, 13).
461 That is, 1) YSU simulates stronger daytime precipitation rate than ACM2 (by 60% at noon time,
462 16 vs. 10 mm day⁻¹, Fig. 13a,b); 2) Stronger boundary layer mixing simulated by YSU with
463 $p=0.5$ leads to more PBL top clouds (Fig. 12c), which block more shortwave radiation and
464 reduce daytime surface temperature and consequently precipitation (with 13 mm day⁻¹ at noon,
465 Fig. 13c); 3) Using the free-troposphere mixing treatment of ACM2 in YSU simulates a more
466 prominent cloud layer at 4-5 km above ground (Fig. 12d) which more effectively blocks
467 shortwave radiation and reduces precipitation (with 11 mm day⁻¹ at noon, Fig. 13d) that is closer
468 to the precipitation rate of ACM2 (Fig. 13b).

469 We repeated our simulations with the scale-aware Grell-Freitas scheme turned on over
470 both 15-km and 3-km domains. The total simulated precipitation is enhanced compared with that
471 using the Tiedtke cumulus scheme (Figure S2-S5 in Supporting Information), which is consistent
472 with our previous study over the southern Great Plains (Hu et al., 2018). The sensitivity of
473 simulated precipitation/clouds to different PBL schemes/treatments (the main focus of this study),
474 however, remains the same (Figure S2-S5 in Supporting Information).

475 **4. Conclusions and discussion**

476 Previous studies by others and a recent study of ours found that precipitation simulations
477 over the Amazon in South America are very sensitive to the PBL scheme used. The exact
478 relationship between the turbulent mixing and precipitation processes in that humid region is,
479 however, not clear. In this study, two-month-long simulations over South America in January-
480 February 2019 are examined to understand the precipitation sensitivity to treatments of turbulent
481 mixing in both the PBL and free troposphere within PBL schemes. Two PBL schemes, the YSU
482 and ACM2 schemes, are the foci of this study since they produced the most and least amount of

483 precipitation among PBL schemes examined. Our results serve to disentangle the turbulence –
484 cloud - precipitation processes over the Amazon and reveal root causes for the sensitivity to PBL
485 schemes, which is a prerequisite for future model improvement. During daytime, while the free-
486 troposphere clouds simulated by YSU dissipate due to solar heating, clouds simulated by ACM2
487 maintains through the day because of enhanced moisture supply due to enhanced *PBL-free-*
488 *troposphere* relay transport process: step 1, enhanced vertical mixing within PBL simulated by
489 ACM2 transports surface moisture to the PBL top where clouds first form, and step 2, enhanced
490 free-troposphere mixing feeds the moisture into the free-troposphere cloud deck. Due to the
491 thicker cloud deck over the Amazon simulated by ACM2, surface radiative heating is reduced
492 and consequently CAPE is reduced. As a result, precipitation is weaker from ACM2. In contrast,
493 the moisture *PBL-free-troposphere* relay transport process simulated by YSU is weaker and the
494 clouds at ~4-5 km dissipate quicker, and CAPE is therefore larger during daytime, leading to
495 more precipitation. To verify the strength of such relay transport process, more advanced
496 observations are warranted, for example, of long-term vertical profiles of cloud mixing
497 ratios. To correctly simulate clouds and precipitation, model performance of reproducing such a
498 moisture relay transport process needs to be carefully evaluated.

499 Two key parameters dictating the vertical mixing in the YSU and ACM2 schemes are
500 identified, which are p , an exponent in the polynomial function determining boundary layer
501 vertical mixing and λ , the asymptotic length scale dictating free-troposphere mixing. Sensitivity
502 simulations with altered p , λ , and other treatments within YSU and ACM2 confirm the
503 sensitivity of precipitation to the mixing strength. Calibrating parameters (p , λ) in YSU and
504 ACM2 or improving their parameterization with non-constant values may be needed for general
505 improvement to simulation results, although this is beyond the scope of this study.

506 The free-troposphere mixing in presence of clouds become prominent (which is
507 otherwise weak) because of reduced moist static stability and the difference in free-troposphere
508 mixing appears to explain more of the sensitivity to the YSU and ACM2 PBL schemes. The
509 turbulent mixing and cloud relationship over the Amazon simulated with ACM2 suggests strong
510 positive feedback through which regions of lower troposphere clouds create conditions favorable
511 for daytime cloud maintenance. Such feedback is weaker with YSU, which leads to daytime
512 breakup of free-troposphere clouds.

513 The above results regarding the turbulence-clouds-precipitation processes and their
514 parameterizations have important implications to the understanding and accurate prediction of
515 weather, climate, as well as air quality over the Amazon region that is humid, cloudy and rich in
516 precipitation. South America is experiencing an increasing trend in summer precipitation ([Adler
517 et al., 2017](#)), and such a trend is also projected by some climate models ([Vera et al., 2006b](#)).
518 Given the negative cloud-precipitation correlation seen in this study for the Amazon region, such
519 a precipitation trend may imply a decreasing trend of cloud cover in the region. Correct
520 representation of turbulence mixing-cloud-radiation interactions within weather and climate
521 models is clearly critical for accurate simulation/prediction of precipitation and water cycles.

522 Though not shown here, the precipitation over Amazon appears to affect the strength of
523 the south American LLJ. The convection over the Amazon produces upward motion that diverts
524 the low-level easterly flows upward. Since simulated precipitation is weaker with ACM2, such
525 upward diversion is less so that easterly winds leaving the Amazon and impinging on the east
526 side of Andes are stronger, leading to stronger southward LLJ east of Andes when the easterly
527 flows are diverted southward by the mountain range. While south American LLJ depends on the
528 subtropical weather patterns, such as the Bolivia high, the Chaco low ([Boers et al., 2015](#);
529 [Montini et al., 2019](#); [Salio et al., 2002](#); [Seiler et al., 2013](#); [Vera et al., 2006a](#)). it is modulated by
530 the convection/turbulence interactions over the Amazon. Thus, the simulated strength of
531 Amazonian precipitation is closely linked to the strength of LLJ east of Andes, which may have
532 implications for the simulation of downstream atmospheric environments including temperature
533 and humidity conditions and air quality ([Hu et al., 2013b](#); [Hu et al., 2013c](#); [Klein et al., 2014](#)).
534 These are topics for future studies.

535

536

537 *Acknowledgments.* This work was primarily supported by grant no. 20163646499 from the
538 Universidad Nacional de San Agustín de Arequipa (UNSA) of Peru through the IREES/LASI
539 Global Change and Human Health Institute. The first author is partially supported by the
540 National Mesonet Program grant #10558200 and DOE ASR project (DE-SC0021159). Ming
541 Xue was also supported by NSF grants AGS-1917701. We are grateful to Bowen Zhou, Lan Gao
542 and Jonathan E. Pleim for discussion. The WRF simulations were performed on supercomputers
543 Stampede 2 at the Texas Advanced Computing Center (TACC) through allocations TG-

544 MCA95C006, and TG-ATM160014 from the Advanced Cyberinfrastructure Coordination
545 Ecosystem: Services & Support (ACCESS) program, which is supported by National Science
546 Foundation grants #2138259, #2138286, #2138307, #2137603, and #2138296. The authors also
547 acknowledge high-performance computing support from Cheyenne
548 (<https://doi.org/10.5065/D6RX99HX>) provided by NCAR's Computational and Information
549 Systems Laboratory. NCAR is sponsored by the National Science Foundation. Some of the post-
550 processing of simulations for this work was performed at the University of Oklahoma (OU)
551 Supercomputing Center for Education and Research (OSCER).

552 *Data Availability Statement.*

553 The ERA5 reanalysis data (Hersbach et al., 2020) are available at
554 <https://doi.org/10.5065/BH6N-5N20>. GPM IMERG Final Precipitation dataset is from
555 Huffman et al. (2019). CMORPH dataset (Joyce et al., 2004) is available at
556 https://ftp.cpc.ncep.noaa.gov/precip/CMORPH_V1.0/CRT/8km-30min (last access: 12 November
557 2020). Figures in this manuscript are produced using the NCAR Command Language (Version
558 6.6.2) [Software] (2019). Model data produced from this study have been archived at CAPS
559 website <https://caps.ou.edu/micronet/Regionalclimate.html> and the Luster NSF projects data
560 server at the San Diego Super computer Center, /expand/luster/projects/uok114/xhu2

561 **References**

- 562 Adebisi, A. A., Zuidema, P., Chang, I., Burton, S. P., & Cairns, B. (2020). Mid-level clouds are
563 frequent above the southeast Atlantic stratocumulus clouds. *Atmos. Chem. Phys.*, *20*(18),
564 11025-11043. 10.5194/acp-20-11025-2020
- 565 Adler, R. F., Gu, G., Sapiano, M., Wang, J.-J., & Huffman, G. J. (2017). Global Precipitation:
566 Means, Variations and Trends During the Satellite Era (1979–2014). *Surveys in*
567 *Geophysics*, *38*(4), 679-699. 10.1007/s10712-017-9416-4
- 568 Angevine, W. M., Eddington, L., Durkee, K., Fairall, C., Bianco, L., & Brioude, J. (2012).
569 Meteorological Model Evaluation for CalNex 2010. *Monthly Weather Review*, *140*(12),
570 3885-3906. 10.1175/Mwr-D-12-00042.1
- 571 Angevine, W. M., Jiang, H. L., & Mauritsen, T. (2010). Performance of an Eddy Diffusivity-
572 Mass Flux Scheme for Shallow Cumulus Boundary Layers. *Monthly Weather Review*,
573 *138*(7), 2895-2912. 10.1175/2010mwr3142.1
- 574 Barber, K. A., Burleyson, C. D., Feng, Z., & Hagos, S. M. (2022). The Influence of Shallow
575 Cloud Populations on Transitions to Deep Convection in the Amazon. *Journal of the*
576 *Atmospheric Sciences*, *79*(3), 723-743. 10.1175/jas-d-21-0141.1

577 Beare, R. J., MacVean, M. K., Holtslag, A. A. M., Cuxart, J., Esau, I., Golaz, J. C., . . . Sullivan,
578 P. (2006). An intercomparison of large-eddy simulations of the stable boundary layer.
579 *Boundary-Layer Meteorology*, 118(2), 247-272. 10.1007/s10546-004-2820-6

580 Boers, N., Barbosa, H. M. J., Bookhagen, B., Marengo, J. A., Marwan, N., & Kurths, J. (2015).
581 Propagation of Strong Rainfall Events from Southeastern South America to the Central
582 Andes. *Journal of Climate*, 28(19), 7641-7658. <https://doi.org/10.1175/JCLI-D-15-0137.1>

583

584 Bright, D. R., & Mullen, S. L. (2002). The sensitivity of the numerical simulation of the
585 southwest monsoon boundary layer to the choice of PBL turbulence parameterization in
586 MM5. *Weather and Forecasting*, 17(1), 99-114. Doi 10.1175/1520-
587 0434(2002)017<0099:Tsofns>2.0.Co;2

588 Burleyson, C. D., & Yuter, S. E. (2015). Patterns of Diurnal Marine Stratocumulus Cloud
589 Fraction Variability. *Journal of Applied Meteorology and Climatology*, 54(4), 847-866.
590 10.1175/jamc-d-14-0178.1

591 Chakraborty, S., Jiang, J. H., Su, H., & Fu, R. (2020). Deep Convective Evolution From Shallow
592 Clouds Over the Amazon and Congo Rainforests. *Journal of Geophysical Research:*
593 *Atmospheres*, 125(1), e2019JD030962. <https://doi.org/10.1029/2019JD030962>

594 Chakraborty, S., Schiro, K. A., Fu, R., & Neelin, J. D. (2018). On the role of aerosols, humidity,
595 and vertical wind shear in the transition of shallow-to-deep convection at the Green
596 Ocean Amazon 2014/5 site. *Atmos. Chem. Phys.*, 18(15), 11135-11148. 10.5194/acp-18-
597 11135-2018

598 Chen, F., & Zhang, Y. (2009). On the coupling strength between the land surface and the
599 atmosphere: From viewpoint of surface exchange coefficients. *Geophysical Research*
600 *Letters*, 36. L10404, 10.1029/2009gl037980

601 Chen, M., Huang, Y., Li, Z., Larico, A. J. M., Xue, M., Hong, Y., . . . Morales, I. Y. (2022).
602 Cross-Examining Precipitation Products by Rain Gauge, Remote Sensing, and WRF
603 Simulations over a South American Region across the Pacific Coast and Andes.
604 *Atmosphere*, 13(10), 1666.

605 Clark, A. J., Coniglio, M. C., Coffey, B. E., Thompson, G., Xue, M., & Kong, F. Y. (2015).
606 Sensitivity of 24-h Forecast Dryline Position and Structure to Boundary Layer
607 Parameterizations in Convection-Allowing WRF Model Simulations. *Weather and*
608 *Forecasting*, 30(3), 613-638. 10.1175/Waf-D-14-00078.1

609 Cohen, A. E., Cavallo, S. M., Coniglio, M. C., & Brooks, H. E. (2015). A Review of Planetary
610 Boundary Layer Parameterization Schemes and Their Sensitivity in Simulating
611 Southeastern US Cold Season Severe Weather Environments. *Weather and Forecasting*,
612 30(3), 591-612. 10.1175/Waf-D-14-00105.1

613 Coniglio, M. C., Correia, J., Marsh, P. T., & Kong, F. Y. (2013). Verification of Convection-
614 Allowing WRF Model Forecasts of the Planetary Boundary Layer Using Sounding
615 Observations. *Weather and Forecasting*, 28(3), 842-862. 10.1175/Waf-D-12-00103.1

616 Cuxart, J., Holtslag, A. A. M., Beare, R. J., Bazile, E., Beljaars, A., Cheng, A., . . . Xu, K. M.
617 (2006). Single-column model intercomparison for a stably stratified atmospheric
618 boundary layer. *Boundary-Layer Meteorology*, 118(2), 273-303. 10.1007/s10546-005-
619 3780-1

620 Durran, D. R., & Klemp, J. B. (1982). On the Effects of Moisture on the Brunt-Väisälä
621 Frequency. *Journal of Atmospheric Sciences*, 39(10), 2152-2158. 10.1175/1520-
622 0469(1982)039<2152:Oteomo>2.0.Co;2

623 Fu, R., Zhu, B., & Dickinson, R. E. (1999). How Do Atmosphere and Land Surface Influence
624 Seasonal Changes of Convection in the Tropical Amazon? *Journal of Climate*, 12(5),
625 1306-1321. 10.1175/1520-0442(1999)012<1306:Hdaals>2.0.Co;2

626 Giangrande, S. E., Feng, Z., Jensen, M. P., Comstock, J. M., Johnson, K. L., Toto, T., . . . Martin,
627 S. T. (2017). Cloud characteristics, thermodynamic controls and radiative impacts during
628 the Observations and Modeling of the Green Ocean Amazon (GoAmazon2014/5)
629 experiment. *Atmos. Chem. Phys.*, 17(23), 14519-14541. 10.5194/acp-17-14519-2017

630 Giangrande, S. E., Wang, D., & Mechem, D. B. (2020). Cloud regimes over the Amazon Basin:
631 perspectives from the GoAmazon2014/5 campaign. *Atmos. Chem. Phys.*, 20(12), 7489-
632 7507. 10.5194/acp-20-7489-2020

633 Gopalakrishnan, D., Taraphdar, S., Pauluis, O. M., Xue, L., Ajayamohan, R. S., Al Shamsi,
634 N., . . . Rasmussen, R. M. (2023). Anatomy of a summertime convective event over the
635 Arabian region. *Monthly Weather Review*. <https://doi.org/10.1175/MWR-D-22-0082.1>

636 Gunwani, P., & Mohan, M. (2017). Sensitivity of WRF model estimates to various PBL
637 parameterizations in different climatic zones over India. *Atmospheric Research*, 194, 43-
638 65. <https://doi.org/10.1016/j.atmosres.2017.04.026>

639 Hersbach, H., Bell, B., Berrisford, P., Hirahara, S., Horányi, A., Muñoz-Sabater, J., . . . Thépaut,
640 J.-N. (2020). The ERA5 global reanalysis. *Quarterly Journal of the Royal Meteorological*
641 *Society*, 146(730), 1999-2049. <https://doi.org/10.1002/qj.3803>

642 Hong, S. Y. (2010). A new stable boundary-layer mixing scheme and its impact on the simulated
643 East Asian summer monsoon. *Quarterly Journal of the Royal Meteorological Society*,
644 136(651), 1481-1496. 10.1002/qj.665

645 Hong, S. Y., Noh, Y., & Dudhia, J. (2006). A new vertical diffusion package with an explicit
646 treatment of entrainment processes. *Monthly Weather Review*, 134(9), 2318-2341. Doi
647 10.1175/Mwr3199.1

648 Hu, X.-M., Doughty, D. C., Sanchez, K. J., Joseph, E., & Fuentes, J. D. (2012). Ozone variability
649 in the atmospheric boundary layer in Maryland and its implications for vertical transport
650 model. *Atmospheric Environment*, 46, 354-364. DOI 10.1016/j.atmosenv.2011.09.054

651 Hu, X.-M., Klein, P. M., & Xue, M. (2013a). Evaluation of the updated YSU planetary boundary
652 layer scheme within WRF for wind resource and air quality assessments. *Journal of*
653 *Geophysical Research-Atmospheres*, 118(18), 10490-10505. 10.1002/jgrd.50823

654 Hu, X.-M., Klein, P. M., Xue, M., Lundquist, J. K., Zhang, F., & Qi, Y. (2013b). Impact of Low-
655 Level Jets on the Nocturnal Urban Heat Island Intensity in Oklahoma City. *Journal of*
656 *Applied Meteorology and Climatology*, 52(8), 1779-1802. 10.1175/jamc-d-12-0256.1

657 Hu, X.-M., Klein, P. M., Xue, M., Zhang, F., Doughty, D. C., Forkel, R., . . . Fuentes, J. D.
658 (2013c). Impact of the vertical mixing induced by low-level jets on boundary layer ozone
659 concentration. *Atmospheric Environment*, 70, 123-130. 10.1016/j.atmosenv.2012.12.046

660 Hu, X.-M., Nielsen-Gammon, J. W., & Zhang, F. Q. (2010a). Evaluation of Three Planetary
661 Boundary Layer Schemes in the WRF Model. *Journal of Applied Meteorology and*
662 *Climatology*, 49(9), 1831-1844. 10.1175/2010jamc2432.1

663 Hu, X.-M., Xue, M., & Li, X. (2019). The Use of High-Resolution Sounding Data to Evaluate
664 and Optimize Nonlocal PBL Schemes for Simulating the Slightly Stable Upper
665 Convective Boundary Layer. *Monthly Weather Review*, 147(10), 3825-3841.
666 10.1175/mwr-d-19-0085.1

- 667 Hu, X.-M., Xue, M., McPherson, R. A., Martin, E., Rosendahl, D. H., & Qiao, L. (2018).
668 Precipitation Dynamical Downscaling Over the Great Plains. *Journal of Advances in*
669 *Modeling Earth Systems*, 10(2), 421-447. 10.1002/2017ms001154
- 670 Hu, X.-M., Zhang, F., & Nielsen-Gammon, J. W. (2010b). Ensemble-based simultaneous state
671 and parameter estimation for treatment of mesoscale model error: A real-data study.
672 *Geophysical Research Letters*, 37. L08802, 10.1029/2010gl043017
- 673 Huang, H. Y., Hall, A., & Teixeira, J. (2013). Evaluation of the WRF PBL Parameterizations for
674 Marine Boundary Layer Clouds: Cumulus and Stratocumulus. *Monthly Weather Review*,
675 141(7), 2265-2271. 10.1175/Mwr-D-12-00292.1
- 676 Huang, Y., Xue, M., Hu, X.-M., Martin, E. R., Novoa, H., & McPherson, R. A. (2021).
677 *Convection-Permitting Regional Climate Simulations over South America and the*
678 *Peruvian Central Andes: Evaluation of Precipitation and MCS Simulations and*
679 *Sensitivity to Physics Parameterizations*. Paper presented at the AGU Fall Meeting, New
680 Orleans, LA, <https://agu2021fallmeeting-agu.ipostersessions.com/?s=A8-A3-C9-83-2A-48-C5-B0-72-9E-E3-46-AD-14-1A-7E>.
681
- 682 Huang, Y., Xue, M., Hu, X.-M., Martin, E. R., Novoa, H., McPherson, R. A., . . . Morales, I. Y.
683 (2023). Convection-Permitting Simulations of Precipitation over the Peruvian Central
684 Andes: Strong Sensitivity to Planetary Boundary Layer Parameterization. *ESS Open*
685 *Archive*. 10.22541/essoar.168500290.09079234/v1
- 686 Huffman, G. J., E.F. Stocker, D.T. Bolvin, Nelkin, E. J., & Tan, J. (2019). GPM IMERG Final
687 Precipitation L3 1 day 0.1 degree x 0.1 degree V06 (Publication no.
688 <https://doi.org/10.5067/GPM/IMERGDF/DAY/06>). Retrieved Nov. 2022
- 689 Iacono, M. J., Delamere, J. S., Mlawer, E. J., Shephard, M. W., Clough, S. A., & Collins, W. D.
690 (2008). Radiative forcing by long-lived greenhouse gases: Calculations with the AER
691 radiative transfer models. *Journal of Geophysical Research: Atmospheres*, 113(D13).
692 <https://doi.org/10.1029/2008JD009944>
- 693 Jankov, I., Gallus, W. A., Segal, M., Shaw, B., & Koch, S. E. (2005). The impact of different
694 WRF model physical parameterizations and their interactions on warm season MCS
695 rainfall. *Weather and Forecasting*, 20(6), 1048-1060. Doi 10.1175/Waf888.1
- 696 Jankov, I., Schultz, P. J., Anderson, C. J., & Koch, S. E. (2007). The Impact of Different
697 Physical Parameterizations and Their Interactions on Cold Season QPF in the American
698 River Basin. *Journal of Hydrometeorology*, 8(5), 1141-1151. 10.1175/jhm630.1
- 699 Jiménez, P. A., Dudhia, J., González-Rouco, J. F., Navarro, J., Montávez, J. P., & García-
700 Bustamante, E. (2012). A Revised Scheme for the WRF Surface Layer Formulation.
701 *Monthly Weather Review*, 140(3), 898-918. 10.1175/mwr-d-11-00056.1
- 702 Joyce, R. J., Janowiak, J. E., Arkin, P. A., & Xie, P. (2004). CMORPH: A Method that Produces
703 Global Precipitation Estimates from Passive Microwave and Infrared Data at High
704 Spatial and Temporal Resolution. *Journal of Hydrometeorology*, 5(3), 487-503.
705 10.1175/1525-7541(2004)005<0487:Camtpg>2.0.Co;2
- 706 Kay, J. E., Bourdages, L., Miller, N. B., Morrison, A., Yettella, V., Chepfer, H., & Eaton, B.
707 (2016). Evaluating and improving cloud phase in the Community Atmosphere Model
708 version 5 using spaceborne lidar observations. *Journal of Geophysical Research:*
709 *Atmospheres*, 121(8), 4162-4176. <https://doi.org/10.1002/2015JD024699>
- 710 Kay, J. E., Hillman, B. R., Klein, S. A., Zhang, Y., Medeiros, B., Pincus, R., . . . Ackerman, T. P.
711 (2012). Exposing Global Cloud Biases in the Community Atmosphere Model (CAM)

712 Using Satellite Observations and Their Corresponding Instrument Simulators. *Journal of*
713 *Climate*, 25(15), 5190-5207. 10.1175/jcli-d-11-00469.1

714 Klein, P. M., Hu, X. M., & Xue, M. (2014). Impacts of Mixing Processes in Nocturnal
715 Atmospheric Boundary Layer on Urban Ozone Concentrations. *Boundary-Layer*
716 *Meteorology*, 150(1), 107-130. 10.1007/s10546-013-9864-4

717 Langenbrunner, B., Pritchard, M. S., Kooperman, G. J., & Randerson, J. T. (2019). Why Does
718 Amazon Precipitation Decrease When Tropical Forests Respond to Increasing CO₂?
719 *Earth's Future*, 7(4), 450-468. <https://doi.org/10.1029/2018EF001026>

720 Li, X. L., & Pu, Z. X. (2008). Sensitivity of Numerical Simulation of Early Rapid Intensification
721 of Hurricane Emily (2005) to Cloud Microphysical and Planetary Boundary Layer
722 Parameterizations. *Monthly Weather Review*, 136(12), 4819-4838.
723 10.1175/2008mwr2366.1

724 Lilly, D. K. (1968). Models of Cloud-Topped Mixed Layers under a Strong Inversion. *Quarterly*
725 *Journal of the Royal Meteorological Society*, 94(401), 292-&. DOI
726 10.1002/qj.49709440106

727 Liu, C., Ikeda, K., Rasmussen, R., Dominguez, F., Prein, A. F., Dudhia, J., & Chen, F. (2022).
728 *An Overview of Two-Decade-Long Convection Permitting Regional Climate*
729 *Downscaling over the Continental South America*. Paper presented at the AGU fall
730 meeting, Chicago, IL, <https://agu.confex.com/agu/fm22/meetingapp.cgi/Paper/1115319>.

731 Liu, M., & Carroll, J. J. (1996). A high-resolution air pollution model suitable for dispersion
732 studies in complex terrain. *Monthly Weather Review*, 124(10), 2396-2409. Doi
733 10.1175/1520-0493(1996)124<2396:Ahrapm>2.0.Co;2

734 Lu, X., & Wang, X. (2019). Improving Hurricane Analyses and Predictions with TCI, IFEX
735 Field Campaign Observations, and CIMSS AMVs Using the Advanced Hybrid Data
736 Assimilation System for HWRF. Part I: What is Missing to Capture the Rapid
737 Intensification of Hurricane Patricia (2015) when HWRF is already Initialized with a
738 More Realistic Analysis? *Monthly Weather Review*, 147(4), 1351-1373. 10.1175/mwr-d-
739 18-0202.1

740 Miguez-Macho, G., Stenchikov, G. L., & Robock, A. (2004). Spectral nudging to eliminate the
741 effects of domain position and geometry in regional climate model simulations. *Journal*
742 *of Geophysical Research-Atmospheres*, 109(D13). D13104, 10.1029/2003jd004495

743 Miguez-Macho, G., Stenchikov, G. L., & Robock, A. (2005). Regional climate simulations over
744 North America: Interaction of local processes with improved large-scale flow. *Journal of*
745 *Climate*, 18(8), 1227-1246. Doi 10.1175/Jcli3369.1

746 Montini, T. L., Jones, C., & Carvalho, L. M. V. (2019). The South American Low-Level Jet: A
747 New Climatology, Variability, and Changes. *Journal of Geophysical Research:*
748 *Atmospheres*, 124(3), 1200-1218. <https://doi.org/10.1029/2018JD029634>

749 Nakanishi, M., & Niino, H. (2006). An Improved Mellor–Yamada Level-3 Model: Its Numerical
750 Stability and Application to a Regional Prediction of Advection Fog. *Boundary-Layer*
751 *Meteorology*, 119(2), 397-407. 10.1007/s10546-005-9030-8

752 NCAR Command Language (Version 6.6.2) [Software]. (2019). Boulder, Colorado:
753 UCAR/NCAR/CISL/TDD. <http://dx.doi.org/10.5065/D6WD3XH5>

754 Nielsen-Gammon, J. W., Hu, X.-M., Zhang, F., & Pleim, J. E. (2010). Evaluation of Planetary
755 Boundary Layer Scheme Sensitivities for the Purpose of Parameter Estimation. *Monthly*
756 *Weather Review*, 138(9), 3400-3417. 10.1175/2010mwr3292.1

757 Noh, Y., Cheon, W. G., Hong, S. Y., & Raasch, S. (2003). Improvement of the K-profile model
758 for the planetary boundary layer based on large eddy simulation data. *Boundary-Layer*
759 *Meteorology*, 107(2), 401-427. Doi 10.1023/A:1022146015946

760 Olson, J. B., Kenyon, J. S., Angevine, W. A., Brown, J. M., Pagowski, M., & Sušelj, K. (2019a).
761 A Description of the MYNN-EDMF Scheme and the Coupling to Other Components in
762 WRF-ARW. <https://doi.org/10.25923/n9wm-be49>

763 Olson, J. B., Kenyon, J. S., Djalalova, I., Bianco, L., Turner, D. D., Pichugina, Y., . . . Cline, J.
764 (2019b). Improving Wind Energy Forecasting through Numerical Weather Prediction
765 Model Development. *Bulletin of the American Meteorological Society*, 100(11), 2201-
766 2220. 10.1175/bams-d-18-0040.1

767 Painemal, D., Xu, K.-M., Cheng, A., Minnis, P., & Palikonda, R. (2015). Mean Structure and
768 Diurnal Cycle of Southeast Atlantic Boundary Layer Clouds: Insights from Satellite
769 Observations and Multiscale Modeling Framework Simulations. *Journal of Climate*,
770 28(1), 324-341. 10.1175/jcli-d-14-00368.1

771 Pergaud, J., Masson, V., Malardel, S., & Couvreux, F. (2009). A parameterization of dry
772 thermals and shallow cumuli for mesoscale numerical weather prediction. *Bound.-Layer*
773 *Meteor.*, 132, 83-106.

774 Pleim, J. E. (2007a). A combined local and nonlocal closure model for the atmospheric boundary
775 layer. Part I: Model description and testing. *Journal of Applied Meteorology and*
776 *Climatology*, 46(9), 1383-1395. 10.1175/Jam2539.1

777 Pleim, J. E. (2007b). A combined local and nonlocal closure model for the atmospheric boundary
778 layer. Part II: Application and evaluation in a mesoscale meteorological model. *Journal*
779 *of Applied Meteorology and Climatology*, 46(9), 1396-1409. 10.1175/Jam2534.1

780 Prein, A. F., Ge, M., Valle, A. R., Wang, D., & Giangrande, S. E. (2022). Towards a Unified
781 Setup to Simulate Mid-Latitude and Tropical Mesoscale Convective Systems at
782 Kilometer-Scales. *Earth and Space Science*, 9(8), e2022EA002295.
783 <https://doi.org/10.1029/2022EA002295>

784 Prein, A. F., Langhans, W., Fossier, G., Ferrone, A., Ban, N., Goergen, K., . . . Leung, R. (2015).
785 A review on regional convection-permitting climate modeling: Demonstrations, prospects,
786 and challenges. *Reviews of Geophysics*, 53(2), 323-361.

787 Prein, A. F., Rasmussen, R. M., Ikeda, K., Liu, C., Clark, M. P., & Holland, G. J. (2017). The
788 future intensification of hourly precipitation extremes. *Nature Clim. Change*, 7(1), 48-52.
789 10.1038/nclimate3168,
790 [http://www.nature.com/nclimate/journal/v7/n1/abs/nclimate3168.html#supplementary-](http://www.nature.com/nclimate/journal/v7/n1/abs/nclimate3168.html#supplementary-information)
791 [information](http://www.nature.com/nclimate/journal/v7/n1/abs/nclimate3168.html#supplementary-information)

792 Salio, P., Nicolini, M., & Saulo, A. C. (2002). Chaco low-level jet events characterization during
793 the austral summer season. *Journal of Geophysical Research: Atmospheres*, 107(D24),
794 ACL 32-31-ACL 32-17. <https://doi.org/10.1029/2001JD001315>

795 Seiler, C., Hutjes, R. W. A., & Kabat, P. (2013). Climate Variability and Trends in Bolivia.
796 *Journal of Applied Meteorology and Climatology*, 52(1), 130-146.
797 <https://doi.org/10.1175/JAMC-D-12-0105.1>

798 Shin, H. H., & Hong, S. Y. (2011). Intercomparison of Planetary Boundary-Layer
799 Parametrizations in the WRF Model for a Single Day from CASES-99. *Boundary-Layer*
800 *Meteorology*, 139(2), 261-281. 10.1007/s10546-010-9583-z

- 801 Skamarock, W. C., & Klemp, J. B. (2008). A time-split nonhydrostatic atmospheric model for
802 weather research and forecasting applications. *Journal of Computational Physics*, 227(7),
803 3465-3485. <http://dx.doi.org/10.1016/j.jcp.2007.01.037>
- 804 Skamarock, W. C., Klemp, J. B., Dudhia, J., Gill, D. O., Liu, Z., Berner, J., . . . Huang, X.-y.
805 (2021). *A Description of the Advanced Research WRF Model Version 4.3*. (NCAR/TN-
806 556+STR). Retrieved from <http://dx.doi.org/10.5065/1dfh-6p97>.
- 807 Sun, X. G., Xue, M., Brotzge, J., McPherson, R. A., Hu, X. M., & Yang, X. Q. (2016). An
808 evaluation of dynamical downscaling of Central Plains summer precipitation using a
809 WRF-based regional climate model at a convection-permitting 4km resolution. *Journal of*
810 *Geophysical Research-Atmospheres*, 121(23), 13801-13825. 10.1002/2016jd024796
- 811 Supinie, T. A., Park, J., Snook, N., Hu, X. M., Brewster, K. A., Xue, M., & Carley, J. R. (2022).
812 Cool-Season Evaluation of FV3-LAM-Based CONUS-Scale Forecasts with Physics
813 Configurations of Experimental RRFS Ensembles. *Monthly Weather Review*, 150(9),
814 2379-2398. 10.1175/mwr-d-21-0331.1
- 815 Tai, S.-L., Feng, Z., Ma, P.-L., Schumacher, C., & Fast, J. D. (2021). Representations of
816 Precipitation Diurnal Cycle in the Amazon as Simulated by Observationally Constrained
817 Cloud-System Resolving and Global Climate Models. *Journal of Advances in Modeling*
818 *Earth Systems*, 13(11), e2021MS002586. <https://doi.org/10.1029/2021MS002586>
- 819 Thompson, G., Field, P. R., Rasmussen, R. M., & Hall, W. D. (2008). Explicit Forecasts of
820 Winter Precipitation Using an Improved Bulk Microphysics Scheme. Part II:
821 Implementation of a New Snow Parameterization. *Monthly Weather Review*, 136(12),
822 5095-5115. 10.1175/2008mwr2387.1
- 823 Tiedtke, M. (1989). A Comprehensive Mass Flux Scheme for Cumulus Parameterization in
824 Large-Scale Models. *Monthly Weather Review*, 117(8), 1779-1800. Doi 10.1175/1520-
825 0493(1989)117<1779:Acmfsf>2.0.Co;2
- 826 Troen, I., & Mahrt, L. (1986). A Simple-Model of the Atmospheric Boundary-Layer - Sensitivity
827 to Surface Evaporation. *Boundary-Layer Meteorology*, 37(1-2), 129-148. Doi
828 10.1007/Bf00122760
- 829 Valappil, V. K., Kedia, S., Dwivedi, A. K., Pokale, S. S., Islam, S., & Khare, M. K. (2023).
830 Assessing the performance of WRF ARW model in simulating heavy rainfall events over
831 the Pune region: in support of operational applications. *Meteorology and Atmospheric*
832 *Physics*, 135(2), 16. 10.1007/s00703-023-00952-7
- 833 Vera, C., Baez, J., Douglas, M., Emmanuel, C. B., Marengo, J., Meitin, J., . . . Zipser, E. (2006a).
834 The South American Low-Level Jet Experiment. *Bulletin of the American*
835 *Meteorological Society*, 87(1), 63-78. <https://doi.org/10.1175/BAMS-87-1-63>
- 836 Vera, C., Silvestri, G., Liebmann, B., & González, P. (2006b). Climate change scenarios for
837 seasonal precipitation in South America from IPCC-AR4 models. *Geophysical Research*
838 *Letters*, 33(13). <https://doi.org/10.1029/2006GL025759>
- 839 Vilà-Guerau de Arellano, J., Wang, X., Pedruzo-Bagazgoitia, X., Sikma, M., Agustí-Panareda,
840 A., Boussetta, S., . . . Gerken, T. (2020). Interactions Between the Amazonian Rainforest
841 and Cumuli Clouds: A Large-Eddy Simulation, High-Resolution ECMWF, and
842 Observational Intercomparison Study. *Journal of Advances in Modeling Earth Systems*,
843 12(7), e2019MS001828. <https://doi.org/10.1029/2019MS001828>
- 844 Wang, J. L., & Kotamarthi, V. R. (2013). Assessment of Dynamical Downscaling in Near-
845 Surface Fields with Different Spectral Nudging Approaches Using the Nested Regional

846 Climate Model (NRCM). *Journal of Applied Meteorology and Climatology*, 52(7), 1576-
847 1591. 10.1175/Jamc-D-12-0302.1

848 Wang, J. X., & Hu, X. M. (2021). Evaluating the Performance of WRF Urban Schemes and PBL
849 Schemes over Dallas-Fort Worth during a Dry Summer and a Wet Summer. *Journal of*
850 *Applied Meteorology and Climatology*, 60(6), 779-798. 10.1175/Jamc-D-19-0195.1

851 Wang, W. G., Shen, X. Y., & Huang, W. Y. (2016). A Comparison of Boundary-Layer
852 Characteristics Simulated Using Different Parametrization Schemes. *Boundary-Layer*
853 *Meteorology*, 161(2), 375-403. 10.1007/s10546-016-0175-4

854 Wright, J. S., Fu, R., Worden, J. R., Chakraborty, S., Clinton, N. E., Risi, C., . . . Yin, L. (2017).
855 Rainforest-initiated wet season onset over the southern Amazon. *Proceedings of the*
856 *National Academy of Sciences*, 114(32), 8481-8486. doi:10.1073/pnas.1621516114

857 Wu, M., Lee, J.-E., Wang, D., & Salameh, M. (2021a). Suppressed Daytime Convection Over
858 the Amazon River. *Journal of Geophysical Research: Atmospheres*, 126(13),
859 e2020JD033627. <https://doi.org/10.1029/2020JD033627>

860 Wu, Z., Li, Y., Li, X., Hu, X.-M., Zhou, G., & Deng, C. (2021b). Influence of Different
861 Planetary Boundary Layer Parameterization Schemes on the Simulation of Precipitation
862 Caused by Southwest China Vortex in Sichuan Basin Based on the WRF Model. *Chinese*
863 *Journal of Atmospheric Sciences*, 45(1), 58. 10.3878/j.issn.1006-9895.2005.19171

864 Xie, B., Fung, J. C. H., Chan, A., & Lau, A. (2012). Evaluation of nonlocal and local planetary
865 boundary layer schemes in the WRF model. *Journal of Geophysical Research:*
866 *Atmospheres*, 117(D12). <https://doi.org/10.1029/2011JD017080>

867 Yang, Y., Hu, X.-M., Gao, S., & Wang, Y. (2019). Sensitivity of WRF simulations with the YSU
868 PBL scheme to the lowest model level height for a sea fog event over the Yellow Sea.
869 *Atmospheric Research*, 215, 253-267. <https://doi.org/10.1016/j.atmosres.2018.09.004>

870 Zhang, D., Wang, Z., & Liu, D. (2010). A global view of midlevel liquid-layer topped stratiform
871 cloud distribution and phase partition from CALIPSO and CloudSat measurements.
872 *Journal of Geophysical Research: Atmospheres*, 115(D4).
873 <https://doi.org/10.1029/2009JD012143>

874 Zhang, Y., Jiang, Y., & Tan, B. (2013). Influences of different PBL schemes on secondary
875 eyewall formation and eyewall replacement cycle in simulated Typhoon Sinlaku (2008).
876 *Acta Meteorologica Sinica*, 27, 322-334. 10.1007/s13351-013-0312-7

877 Zhu, P., Hazelton, A., Zhang, Z., Marks, F. D., & Tallapragada, V. (2021). The Role of Eyewall
878 Turbulent Transport in the Pathway to Intensification of Tropical Cyclones. *Journal of*
879 *Geophysical Research: Atmospheres*, 126(17), e2021JD034983.
880 <https://doi.org/10.1029/2021JD034983>

881 Zhu, P., Tyner, B., Zhang, J. A., Aligo, E., Gopalakrishnan, S., Marks, F. D., . . . Tallapragada, V.
882 (2019). Role of eyewall and rainband eddy forcing in tropical cyclone intensification.
883 *Atmos. Chem. Phys.*, 19(22), 14289-14310. 10.5194/acp-19-14289-2019

884

885

886 Table 1. Model configuration for sensitivity simulations modifying parameters and treatments in
 887 the YSU and ACM2 PBL schemes. p is an exponent in the polynomial function determining
 888 vertical mixing strength in the PBL, λ is the asymptotic length scale.

PBL	Grid spacings	Experiment name	Changed parameters/treatments
YSU	15 km	YSU	$p=2$ (default)
		YSUp. 5	$p=0.5$
		YSUuseACM2free	Use free troposphere treatment from ACM2
		YSUp. 5useACM2free	$p=0.5$ & use free troposphere treatment from ACM2
	3km	3kmYSU	$p=2$ (default)
		3kmYSUp. 5	$p=0.5$
3kmYSUp. 5useACM2free		$p=0.5$ & use free troposphere treatment from ACM2	
ACM2	15 km	ACM2	$\lambda=80$ (default)
		ACM2 λ 30	$\lambda=30$
	3 km	3kmACM2	$\lambda=80$ (default)

889
890

891 **Figures**

892 Figure 1. Daily mean precipitation rate in Jan-Feb 2019 simulated with (a) YSU in domain 1, (b)
 893 ACM2 in domain 1 with a 15 km grid spacing, (c) YSU in domain 2, (d) ACM2 in domain 2
 894 with a 3 km grid spacing, (e) single-domain YSU, (f) single-domain ACM2 with a 3 km grid
 895 spacing and from (g) IMERG, (h) CMORPH data. The rectangle in (a) marks the location of the
 896 nested domain.

897
898 Figure 2. Mean precipitation rate over the Amazon in Jan-Feb 2019 from (left) CMORPH, and
 899 simulated by (middle) YSU and (right) ACM2 at (top to bottom) 11, 14, 18, and 21 UTC (7, 10,
 900 14, 17 LST correspondingly).

901
902 Figure 3. Hourly mean precipitation rate at 18 UTC (14 LST) in Jan-Feb 2019 simulated with (a)
 903 YSU in domain 1, (b) ACM2 in domain 1, (c) YSU in domain 2, (d) ACM2 in domain 2, (e)
 904 single-domain YSU, (f) single-domain ACM2 and observed from (g) IMERG, (h) CMORPH.

905
906 Figure 4. Average surface temperature at 17 UTC in Jan-Feb 2019 from (a,c,e) YSU, (b,d,f)
 907 ACM2, and (g,h,i) their difference (ACM2-YSU) in (top to bottom) different domains. The
 908 average difference over land is marked at the lower-left corner in (g,h,i)

909
910 Figure 5. Average surface downward shortwave radiation at 17 UTC in Jan-Feb 2019 simulated
 911 with (a,c,e) YSU, (b,d,f) ACM2, (g,h,i) their difference, and (j,k,l) column-average cloud water
 912 mixing ratios in (top to bottom) different domains. The straight dash lines mark the location of
 913 cross-sections in Figs. 5, 6, and 11.

914

915 Figure 6. Averaged cross-section of cloud water over the Amazon of each day in Jan-Feb 2019
916 simulated by (left) YSU and (right) ACM2 at (a,b) 11, (c,d) 14, (e,f) 17, and (g,h) 21 UTC (7, 10,
917 13, 17 LST correspondingly). The location of these cross-sections is marked in Fig. 5j. The
918 dashed black line and continuous blue line indicate PBL top and terrain surface.

919
920 Figure 7. Cross-section of cloud water over the Amazon in Jan-Feb 2019 simulated by (a) YSU
921 and (b) ACM2, (c) *YSUp.5*, (d) *YSUuseACM2free*, (e) *YSUp.5useACM2free*, (f) *ACM2λ30* at 17
922 UTC. The location of these cross-sections is marked in Fig. 5j

923
924 Figure 8. Average surface downward shortwave radiation at 17 UTC during January-February
925 2019 simulated by (a) YSU, (b) ACM2 and 4 sensitivity simulations (c) *YSUp.5*, (d)
926 *YSUuseACM2free*, (e) *YSUp.5useACM2free*, (f) *ACM2λ30*.

927
928 Figure 9. Average CAPE at 17 UTC during January-February 2019 simulated by (a) YSU, (b)
929 ACM2 and 4 sensitivity simulations (c) *YSUp.5*, (d) *YSUuseACM2free*, (e) *YSUp.5useACM2free*,
930 (f) *ACM2λ30*.

931
932 Figure 10. Mean profiles of (a) vertical moisture flux, (b) water vapor difference from that
933 simulated by YSU, (c) cloud water mixing ratio (Q_{CLOUD}), and (d) vertical mixing coefficient
934 (K_z) at 17 UTC during January-February 2019 at Manaus (location marked in Fig. 9b) simulated
935 by YSU, ACM2 and 4 sensitivity simulations *YSUp.5*, *YSUuseACM2free*, *YSUp.5useACM2free*,
936 *ACM2λ30*.

937
938 Figure 11. Average precipitation rate at 18 UTC during January-February 2019 simulated by (a)
939 YSU, (b) ACM2 and 4 sensitivity simulations (c) *YSUp.5*, (d) *YSUuseACM2free*, (e)
940 *YSUp.5useACM2free*, (f) *ACM2λ30*.

941
942 Figure 12. Cross-section of average noon-time cloud water mixing ratios over the Amazon in
943 Jan-Feb 2019 simulated by (a) *3kmYSU*, (b) *3kmACM2*, (c) *3kmYSUp.5*, and (d)
944 *3kmYSUp.5useACM2free*. The location of these cross-sections is marked in Fig. 5l

945
946 Figure 13. Average noon-time precipitation rate in Jan-Feb 2019 simulated by (a) *3kmYSU*, (b)
947 *3kmACM2*, (c) *3kmYSUp.5*, and (d) *3kmYSUp.5useACM2free*. The domain-averaged values are
948 marked.

949

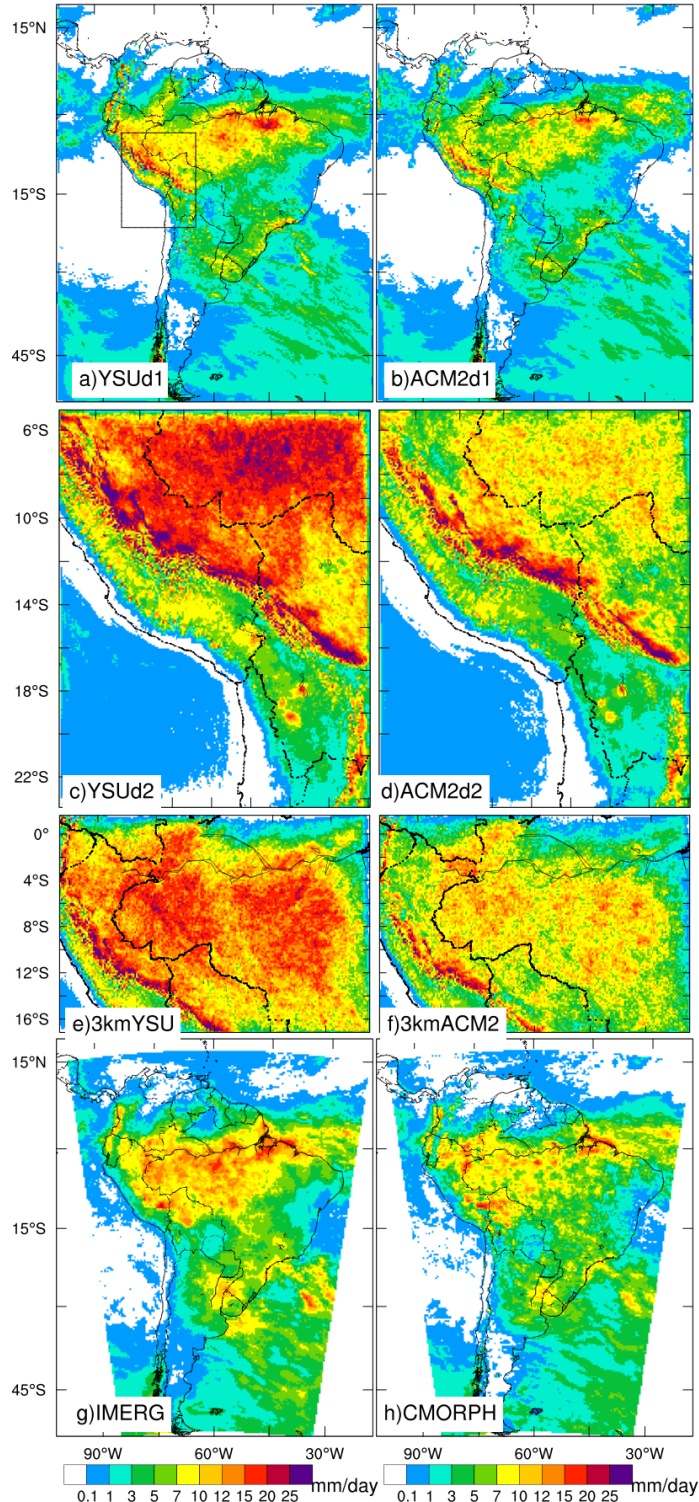


Figure 1. Daily mean precipitation rate in Jan-Feb 2019 simulated with (a) YSU in domain 1, (b) ACM2 in domain 1 with a 15 km grid spacing, (c) YSU in domain 2, (d) ACM2 in domain 2 with a 3 km grid spacing, (e) single-domain YSU, (f) single-domain ACM2 with a 3 km grid spacing and from (g) IMERG, (h) CMORPH data. The rectangle in (a) marks the location of the nested domain.

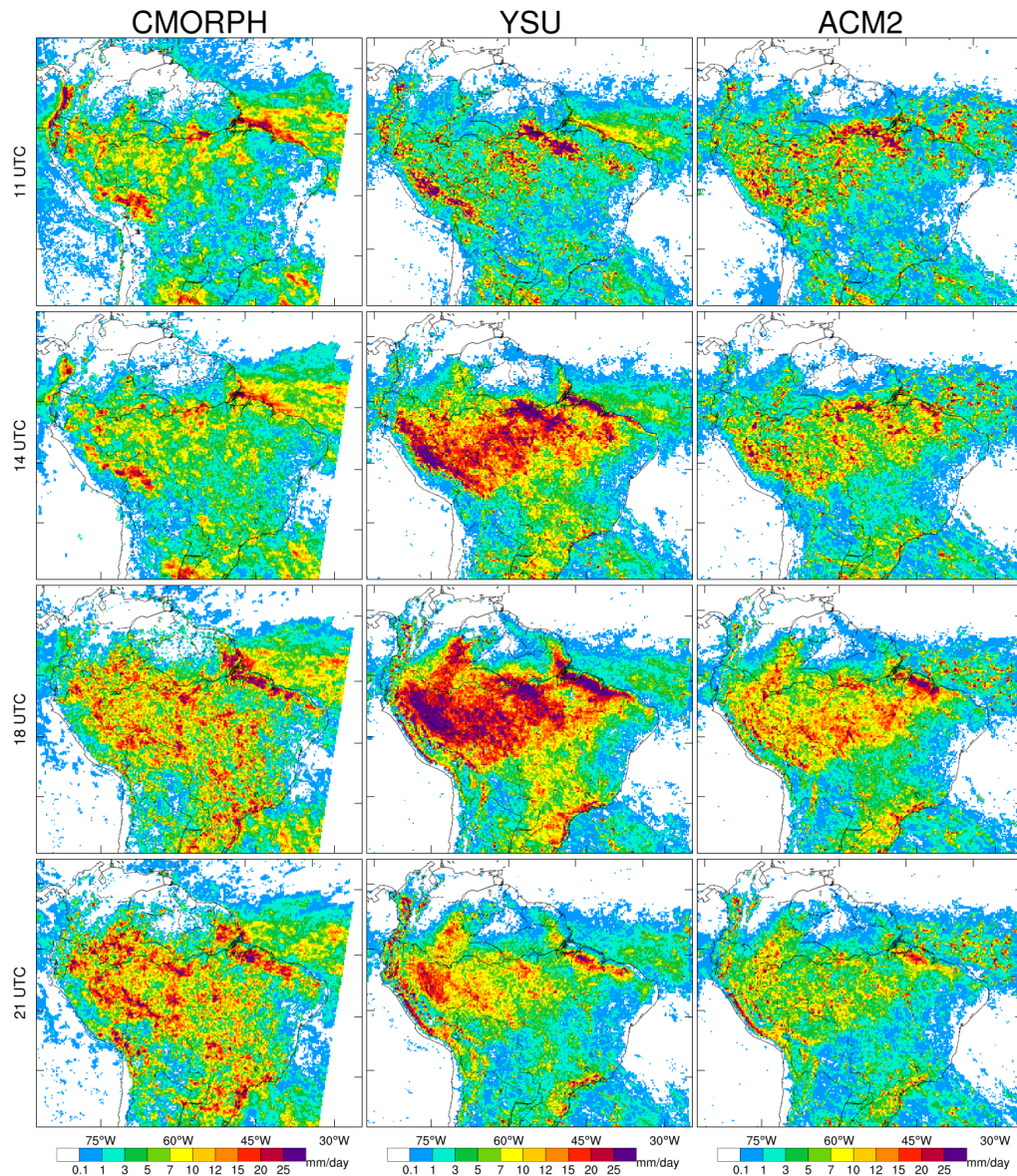


Figure 2. Mean precipitation rate over the Amazon in Jan-Feb 2019 from (left) CMORPH, and simulated by (middle) YSU and (right) ACM2 at (top to bottom) 11, 14, 18, and 21 UTC (7, 10, 14, 17 LST correspondingly).

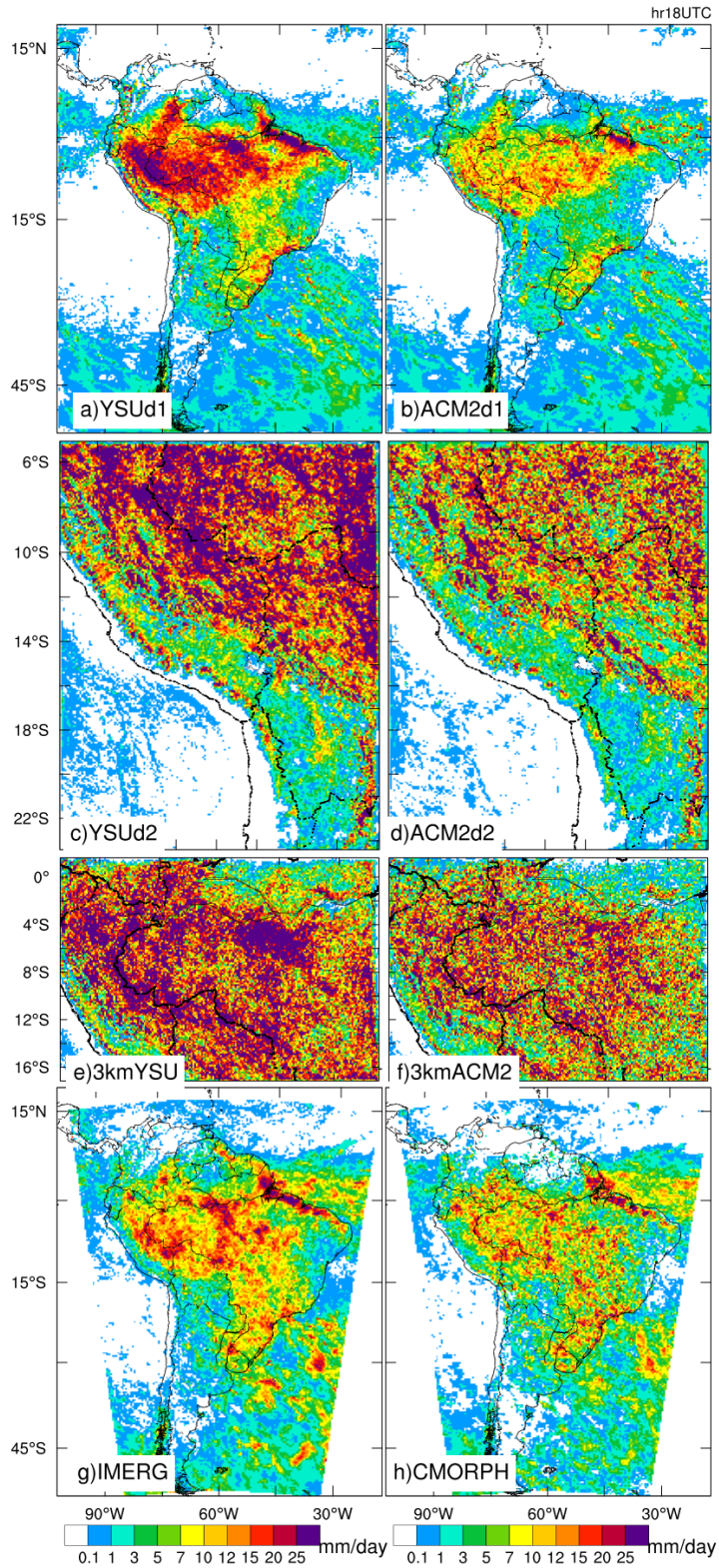


Figure 3. Hourly mean precipitation rate at 18 UTC (14 LST) in Jan-Feb 2019 simulated with (a) YSU in domain 1, (b) ACM2 in domain 1, (c) YSU in domain 2, (d) ACM2 in domain 2, (e) single-domain YSU, (f) single-domain ACM2 and observed from (g) IMERG, (h) CMORPH.

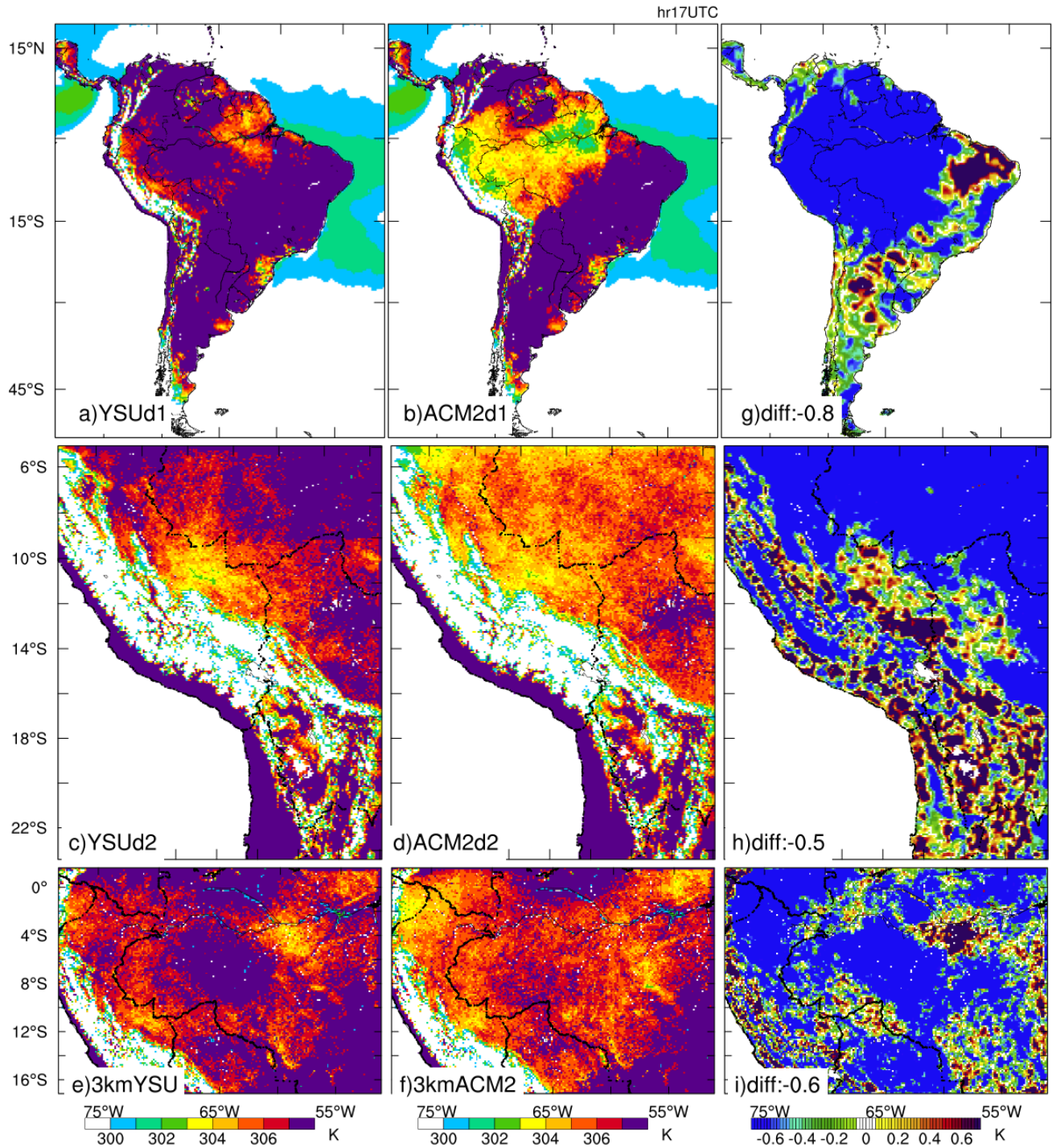


Figure 4. Average surface temperature at 17 UTC in Jan-Feb 2019 from (a,c,e) YSU, (b,d,f) ACM2, and (g,h,i) their difference (ACM2-YSU) in (top to bottom) different domains. The average difference over land is marked at the lower-left corner in (g,h,i)

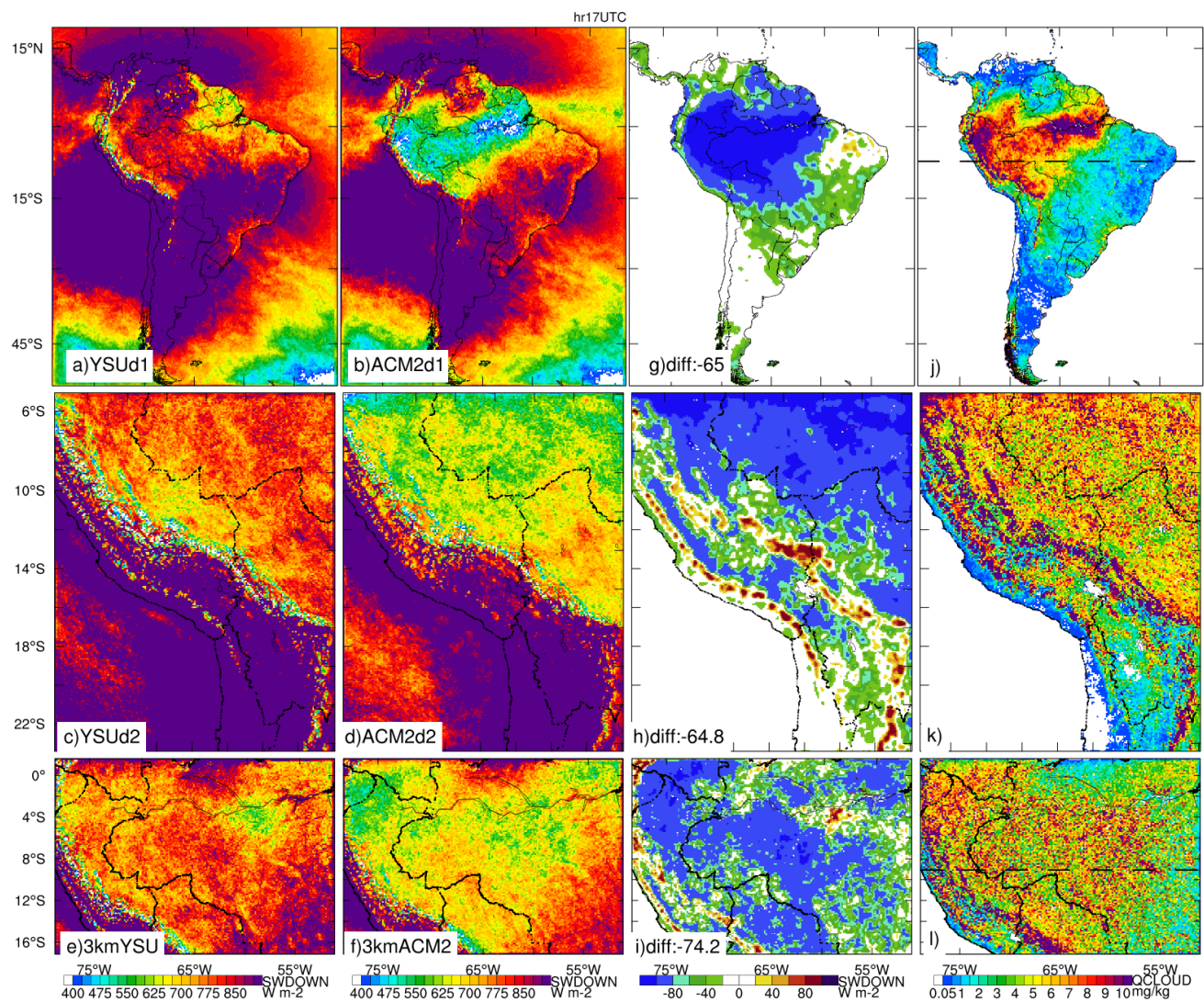


Figure 5. Average surface downward shortwave radiation at 17 UTC in Jan-Feb 2019 simulated with (a,c,e) YSU, (b,d,f) ACM2, (g,h,i) their difference, and (j,k,l) column-average cloud water mixing ratios in (top to bottom) different domains. The straight dash lines mark the location of cross-sections in Figs. 5, 6, and 11.

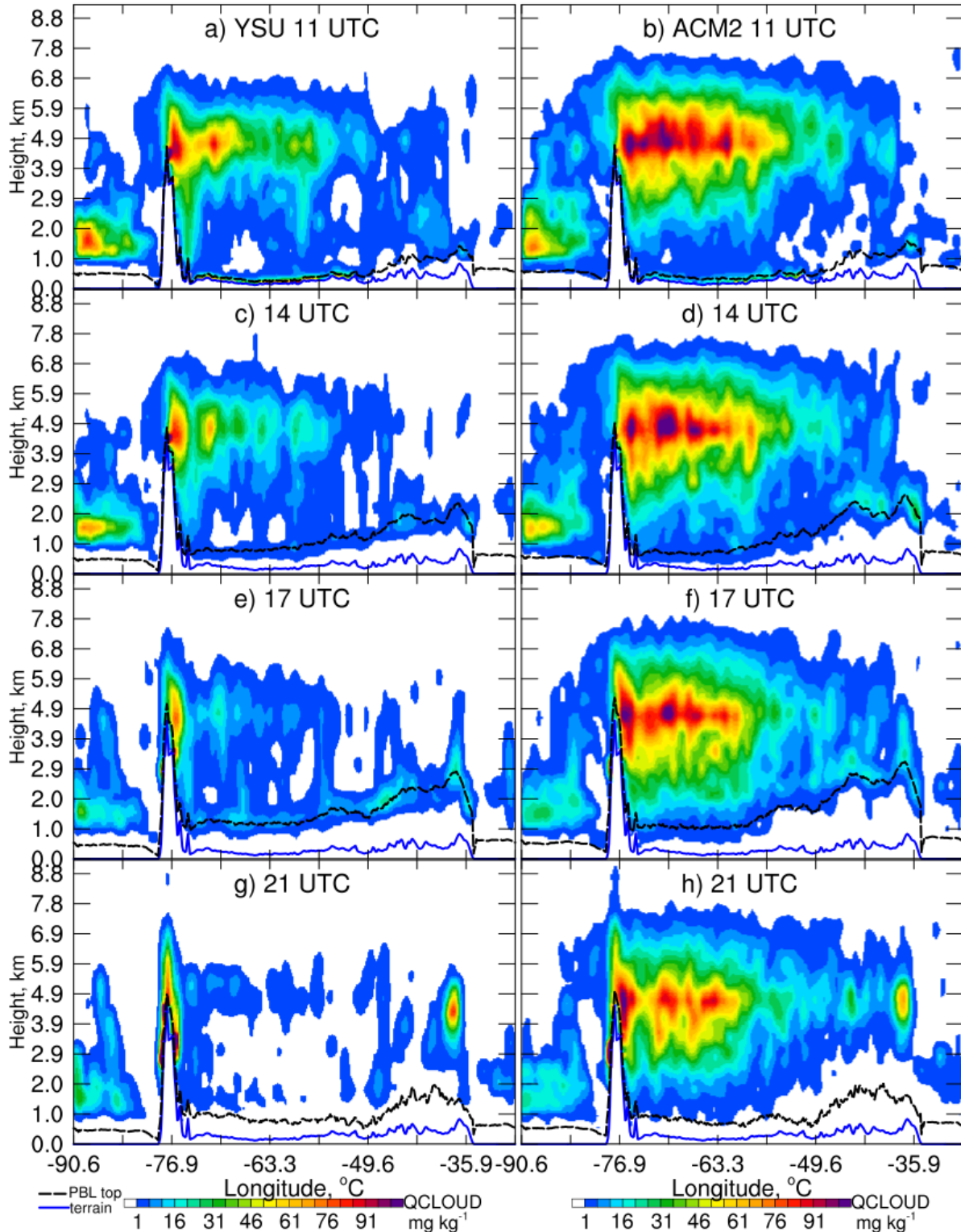


Figure 6. Averaged cross-section of cloud water over the Amazon of each day in Jan-Feb 2019 simulated by (left) YSU and (right) ACM2 at (a,b) 11, (c,d) 14, (e,f) 17, and (g,h) 21 UTC (7, 10, 13, 17 LST correspondingly). The location of these cross-sections is marked in Fig. 5j. The dashed black line and continuous blue line indicate PBL top and terrain surface.

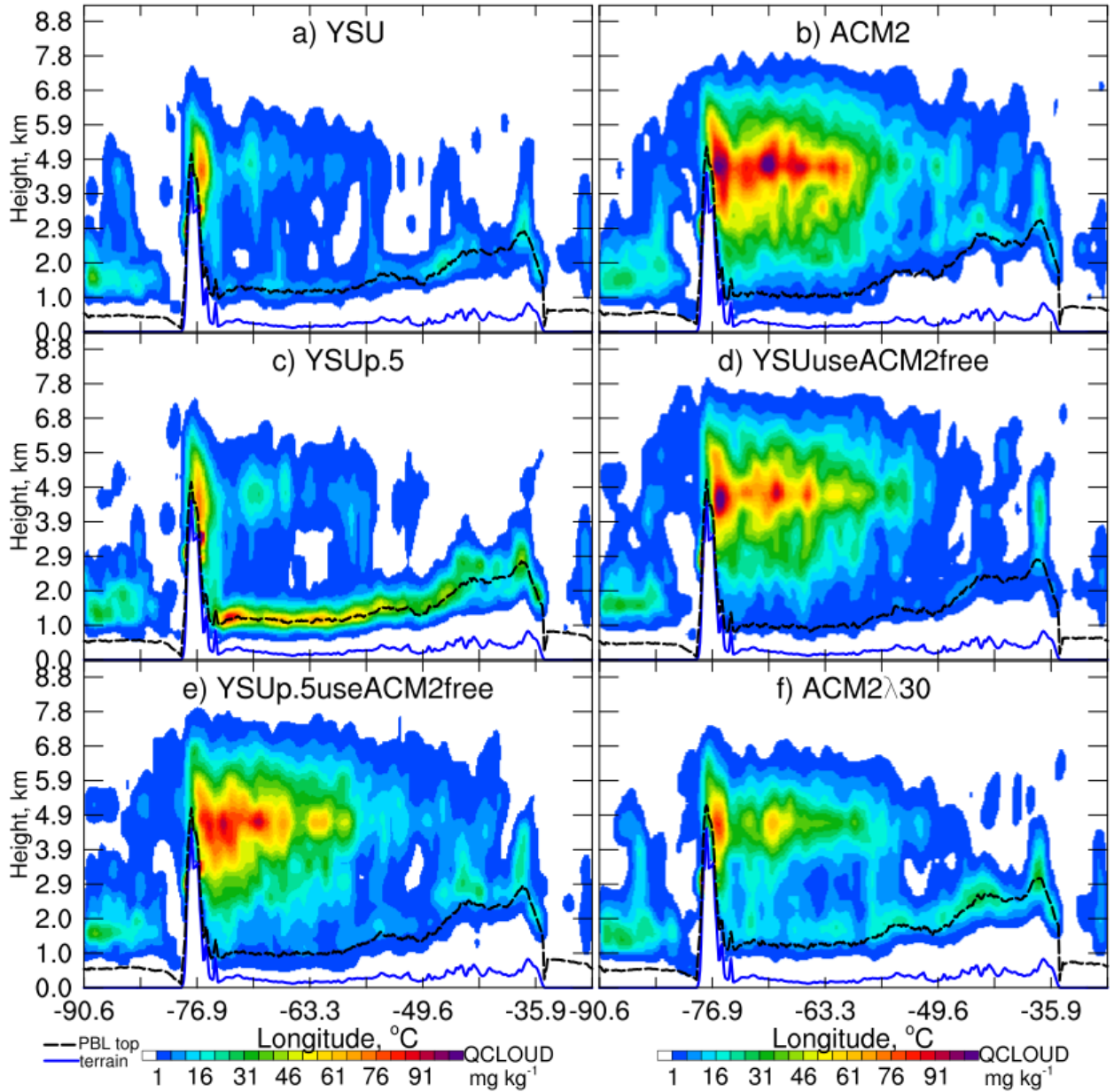


Figure 7. Cross-section of cloud water over the Amazon in Jan-Feb 2019 simulated by (a) YSU and (b) ACM2, (c) YSU_{p.5}, (d) YSU_{useACM2free}, (e) YSU_{p.5useACM2free}, (f) ACM2 λ 30 at 17 UTC. The location of these cross-sections is marked in Fig. 5j

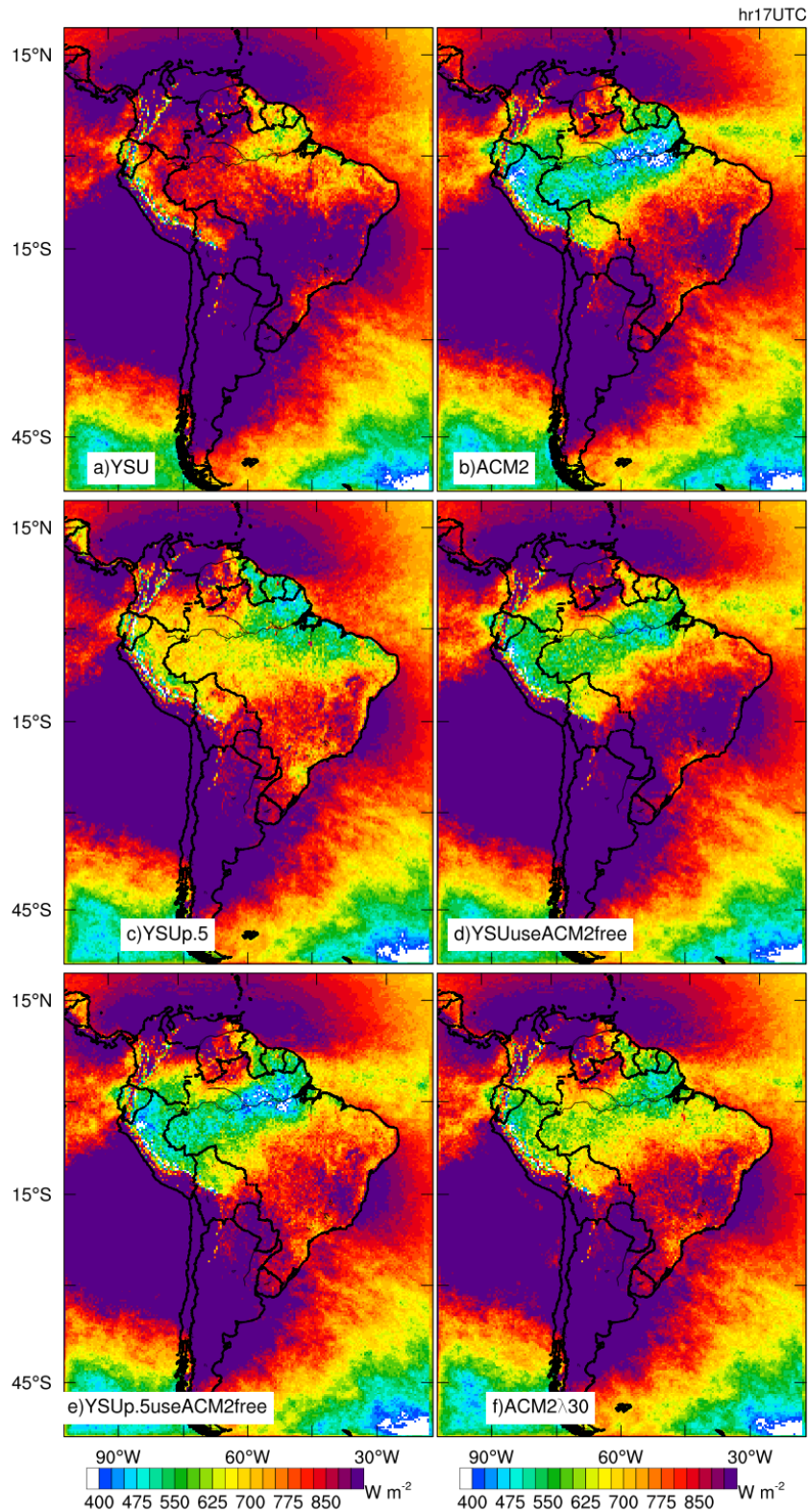


Figure 8. Average surface downward shortwave radiation at 17 UTC during January-February 2019 simulated by (a) YSU, (b) ACM2 and 4 sensitivity simulations (c) YSU p.5 , (d) YSU use ACM2 free, (e) YSU p.5 use ACM2 free, (f) ACM2 $\lambda 30$.

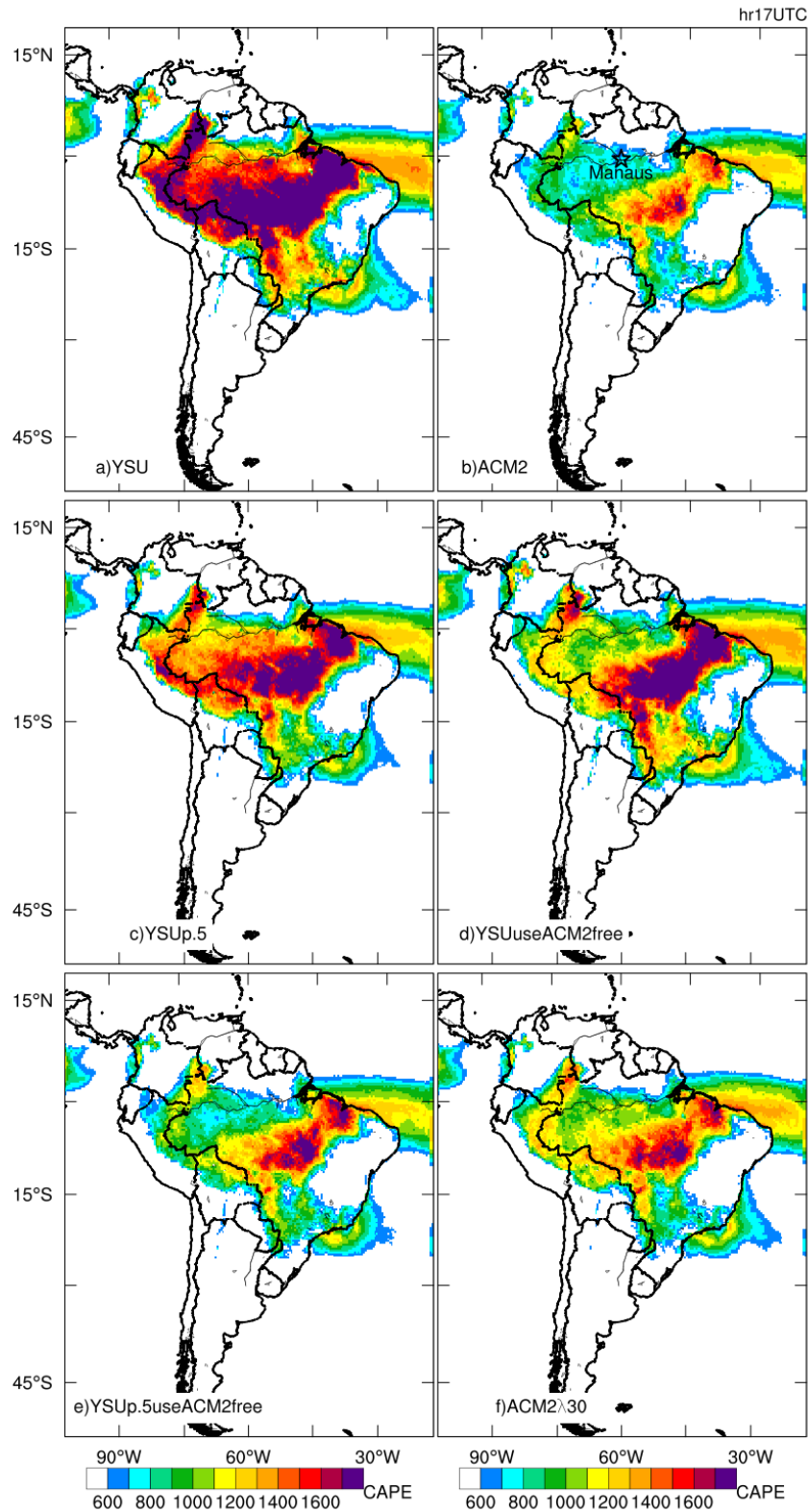


Figure 9. Average CAPE at 17 UTC during January-February 2019 simulated by (a) YSU, (b) ACM2 and 4 sensitivity simulations (c) YSU_{p.5}, (d) YSU_{useACM2free}, (e) YSU_{p.5useACM2free}, (f) ACM2_{λ30}.

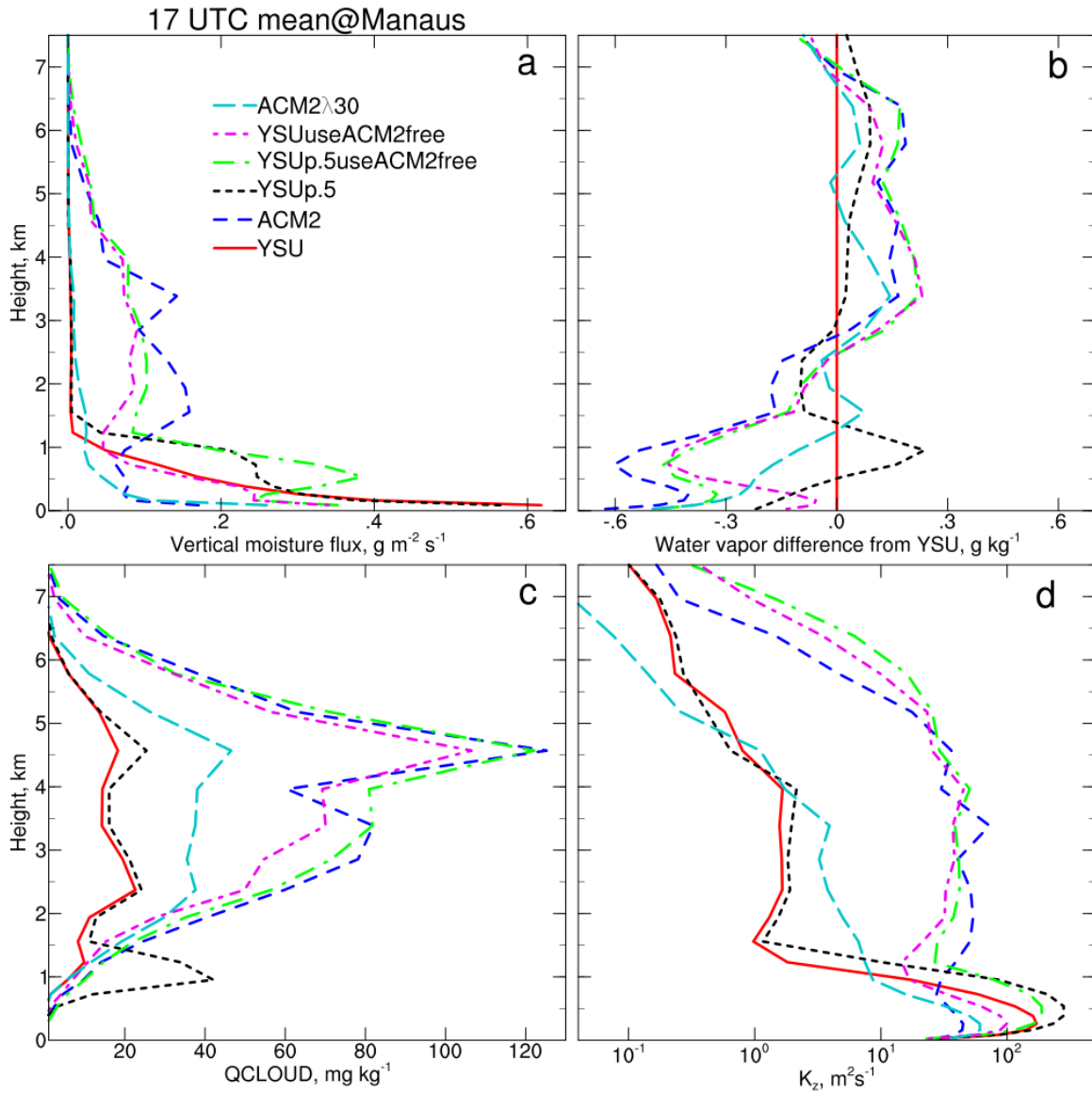


Figure 10. Mean profiles of (a) vertical moisture flux, (b) water vapor difference from that simulated by YSU, (c) cloud water mixing ratio (Q_CLOUD), and (d) vertical mixing coefficient (K_z) at 17 UTC during January-February 2019 at Manaus (location marked in Fig. 9b) simulated by YSU, ACM2 and 4 sensitivity simulations YSUp.5, YSUuseACM2free, YSUp.5useACM2free, ACM2 λ 30.

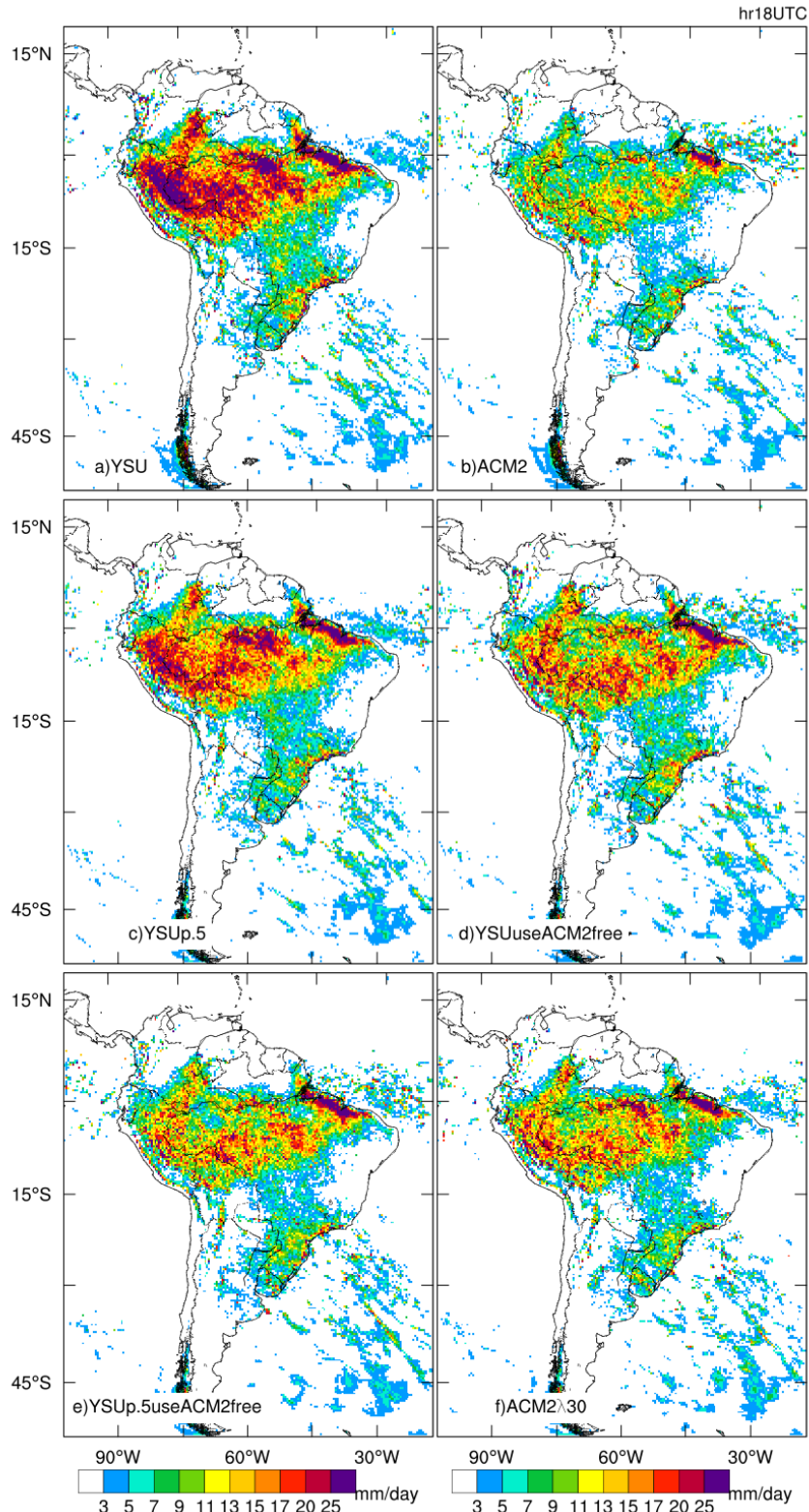


Figure 11. Average precipitation rate at 18 UTC during January-February 2019 simulated by (a) YSU, (b) ACM2 and 4 sensitivity simulations (c) YSU p.5 , (d) YSU use ACM2 free , (e) YSU p.5 use ACM2 free, (f) ACM2 λ 30.

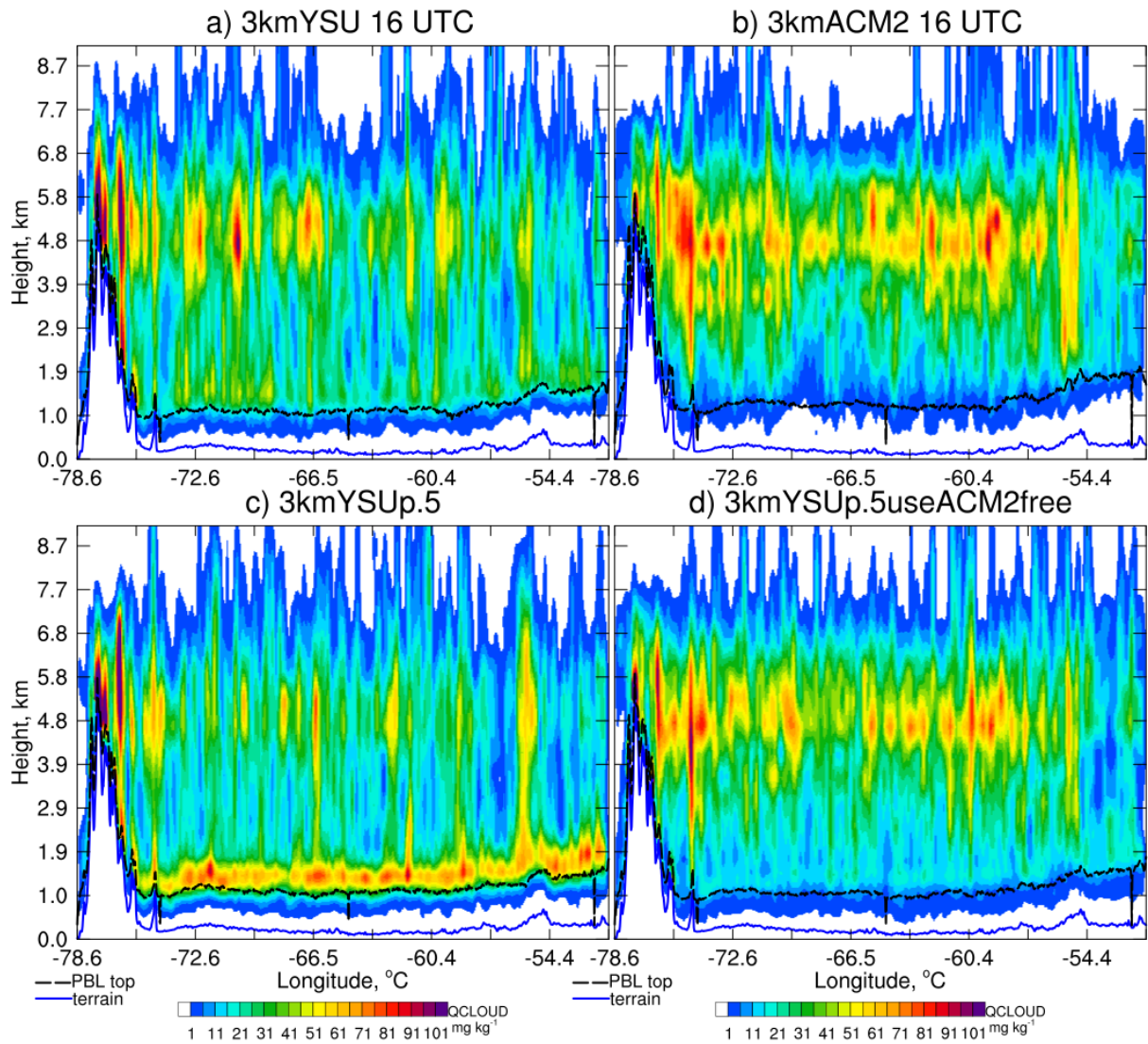


Figure 12. Cross-section of average noon-time cloud water mixing ratios over the Amazon in Jan-Feb 2019 simulated by (a) 3kmYSU , (b) 3kmACM2 , (c) 3kmYSUp.5 , and (d) 3kmYSUp.5useACM2free. The location of these cross-sections is marked in Fig. 51

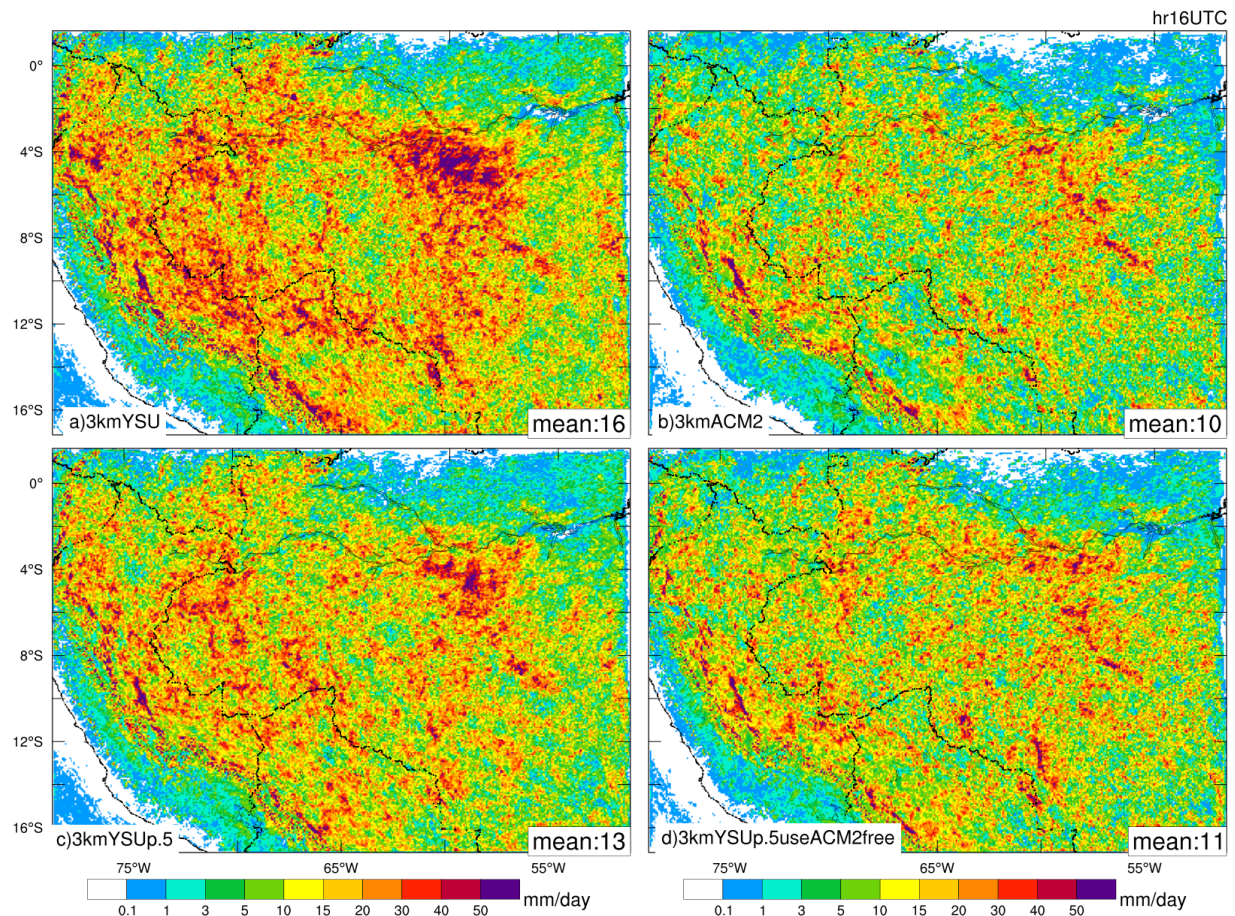


Figure 13. Average noon-time precipitation rate in Jan-Feb 2019 simulated by (a) 3kmYSU, (b) 3kmACM2, (c) 3kmYSUp.5, and (d) 3kmYSUp.5useACM2free. The domain-averaged values are marked.